3. Results

3.1. Role of TRPC channels in smooth muscle cells

3.1.1. Role of TRPC channels in A7r5 smooth muscle cells

3.1.1.1. Vasopressin-induced Ca^{2+} signals in A7r5 cells

To compare the effects of [Arg^8]-vasopressin (AVP) application on $[Ca^{2+}]_i$ of single A7r5 cells with previous studies on this cell type (Byron & Taylor, 1995; Nakajima *et al*., 1996; Broad *et al*., 1999), ratiometric imaging experiments with the Ca^{2+}-sensitive dye fura-2 were performed. In the presence of extracellular Ca^{2+}, addition of AVP (100 nM; $n = 178/178$) to the extracellular solution elicited a substantial increase in F_{340}/F_{380} consisting of a fast rise and a slower decline to baseline (Fig. 7*A*). The slow component of response decay was very heterogeneous in different cells. Some cells exhibited a clear plateau phase ($n = 112/178$, also see *inset* of Fig. 7*A*) whereas in others $[Ca^{2+}]_i$ returned to baseline monophasically ($n = 66/178$, also see *inset* of Fig. 7*A*). Removal of the agonist did not notably affect the rate of decline. In addition to AVP, endothelin I (100 nM; $n = 89/116$), ATP (100 µM; $n = 68/78$), and angiotensin II (100 nM; $n = 16/38$) increased $[Ca^{2+}]_i$ in A7r5 smooth muscle cells, whereas noradrenaline (100 µM; $n = 76$) and the thromboxane A_2 mimetic U46619 (10 µM; $n = 20$) were not effective.

Since the present study was designed to examine the role of TRPC channels in receptor-stimulated Ca^{2+} entry in A7r5 cells, different protocols were used to clarify the contribution of Ca^{2+} release and Ca^{2+} entry across the plasma membrane to the AVP-induced $[Ca^{2+}]_i$ increase depicted in Fig. 7*A*. Many Ca^{2+}-permeable channels, including heterologously-expressed TRPC channels (Hofmann *et al*., 1999; Schaefer *et al*., 2000; Schaefer *et al*., 2002), are permeable to manganese (Mn^{2+}). In one set of experiments, Mn^{2+} was used as a Ca^{2+} surrogate (for details see Materials & Methods) and fura-2 fluorescence was recorded after excitation at the isosbestic wavelength (Fig. 7*B*). The addition of 1 mM Mn^{2+} to the bath had little effect on fura-2 fluorescence, suggesting that the basal rate of Mn^{2+} entry into resting cells is negligible. Subsequent addition of AVP, however, resulted in an immediate, prominent decrease in fluorescence intensity

which stopped as soon as Mn^{2+} was removed from the bath suggesting that AVP activated a Mn^{2+}-permeable cation entry pathway ($n = 148$). Interestingly, Mn^{2+} inhibited the Ca^{2+} response ($n = 119/124$, Fig. 7*B*, *inset*) which was recorded simultanously. In another set of experiments, the effects of Ca^{2+} removal from the bath solution on response amplitude and kinetics were studied (Fig. 7*C,D*). In the absence of extracellular Ca^{2+}, AVP was still able to increase $[Ca^{2+}]_i$, suggesting that Ca^{2+} release contributed to the observed Ca^{2+} response ($n = 162$). However, the response kinetics were changed. The increase in $[Ca^{2+}]_i$ was now followed by a rapid return to prestimulation levels. If, in the continued presence of AVP, Ca^{2+} was added to the bath solution, an increase in F_{340}/F_{380} was observed ($n = 113$). Hence, in addition to Ca^{2+} release, Ca^{2+} entry was involved in AVP-induced Ca^{2+} signalling in A7r5 cells. As expected for a Ca^{2+}-permeable entry pathway, raising the external Ca^{2+} concentration above physiological levels, led to a further increase in $[Ca^{2+}]_i$ presumbly resulting from enhanced influx across the plasma membrane (Fig. 7*D*).

Interestingly, previous studies by Taylor and colleagues (Byron & Taylor, 1995; Broad *et al*., 1999) suggested that Ca^{2+} entry into A7r5 cells involves a capacitative and a non-capacitative component. The store-operated Ca^{2+} entry pathway was suggested to be permeable to Mn^{2+} (but not Sr^{2+}) and irreversibly inhibited by low concentrations of Gd^{3+} (1 μM), whereas the store depletion-independent pathway was permeable to Sr^{2+} (but not to Mn^{2+}) and less sensitive to Gd^{3+} (Broad *et al*., 1999). In contrast, in the present study, only about one half of the cells studied showed enhanced Ca^{2+} influx upon store depletion with thapsigargin and ionomycin ($n = 71/150$, *data not shown*), and this Ca^{2+} influx component was much less pronounced than that described in the above studies. Furthermore, AVP was not found to promote significant Sr^{2+} entry into A7r5 cells ($n = 149$, *data not shown*). A7r5 cells, kindly provided by Dr. Colin Taylor, were found to be indistinguishable in their $[Ca^{2+}]_i$ and current responses to cells obtained from ATCC.

Taken together, the above findings indicate that AVP increases the plasma membrane permeability for divalent cations in A7r5 smooth muscle cells. This Ca^{2+} entry pathway does not depend on L-type voltage-gated Ca^{2+} channels because all experiments were performed in the presence of nimodipine (10 μM), a specific blocker of L-type voltage-

gated Ca^{2+} channels. It is noteworthy, that addition or removal of nimodipine during agonist stimulation did not change the slow, i.e. the Ca^{2+} entry component, of the response (n = 65, Fig. 8*A*). In the absence of nimodipine, elevation of extracellular K^+ to depolarize the cells did not increase $[Ca^{2+}]_i$ above resting levels (n = 12, Fig. 8*B*). These results suggest that, under the experimental conditions used, the contribution of voltage-gated Ca^{2+} channels to AVP-stimulated Ca^{2+} entry in A7r5 smooth muscle cells is negligible.

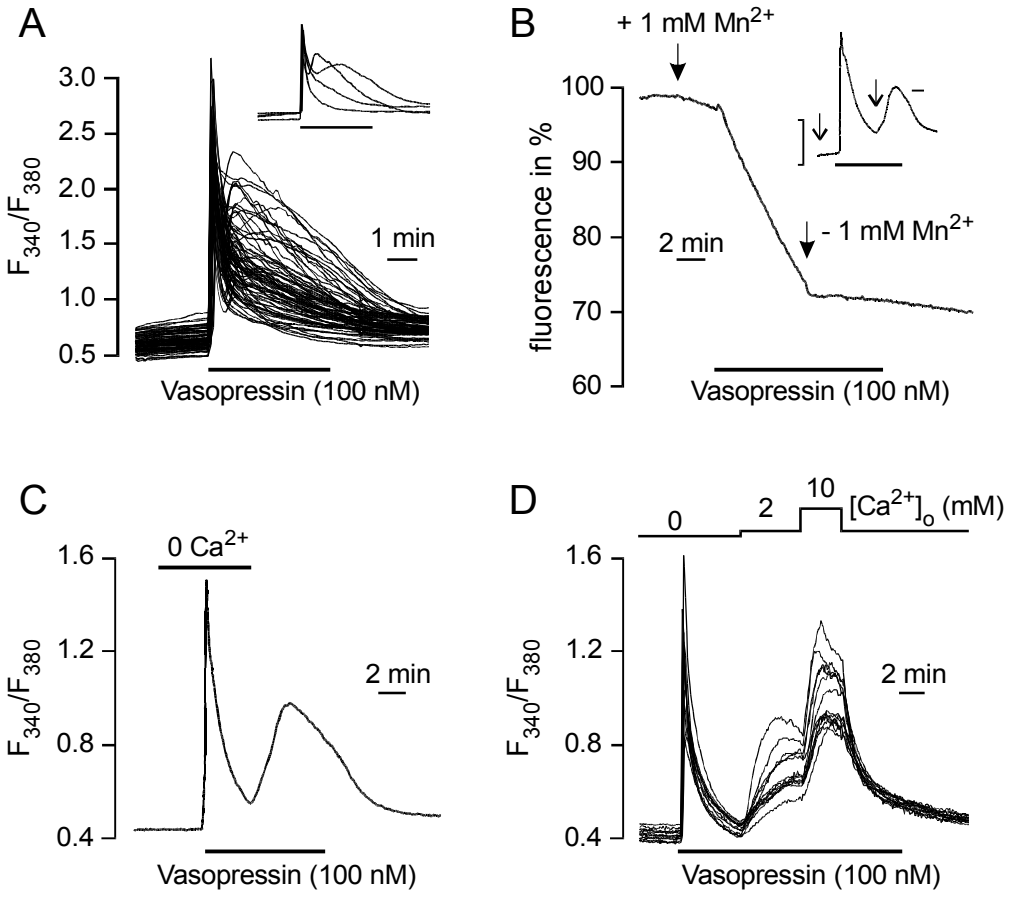

Fig. 7: **Vasopressin-induced Ca^{2+} signalling in A7r5 smooth muscle cells.** *A*: Time-dependent changes in $[Ca^{2+}]_i$ (revealed by changes in fluorescence ratio F_{340}/F_{380}) of individual, fura-2-loaded A7r5 smooth muscle cells upon application of AVP (100 nM). *Inset:* selected traces extracted from *A*. *B*: AVP-induced Mn^{2+} entry into A7r5 cells. The trace is the mean of 15 cells. *Inset*: Simultaneous recording of the effect of Mn^{2+} on changes in $[Ca^{2+}]_i$. *time scale bar*: 2 min, *vertical axis*: F_{340}/F_{380} (0.3 – 0.5). *C,D*: Removal and readdition of Ca_o^{2+} (at varying concentrations) during AVP application. The trace in *C* is the mean of 22 cells.

3.1.1.2. Electrophysiological recordings

Voltage-gated Ca^{2+} channels in A7r5 cells

In view of the intriguing absence of a contribution of voltage-gated Ca^{2+} channels to the AVP-induced Ca^{2+} response in Ca^{2+} imaging experiments, whole-cell patch clamp recordings were performed to evaluate the role of voltage-gated Ca^{2+} channels in this cell line.

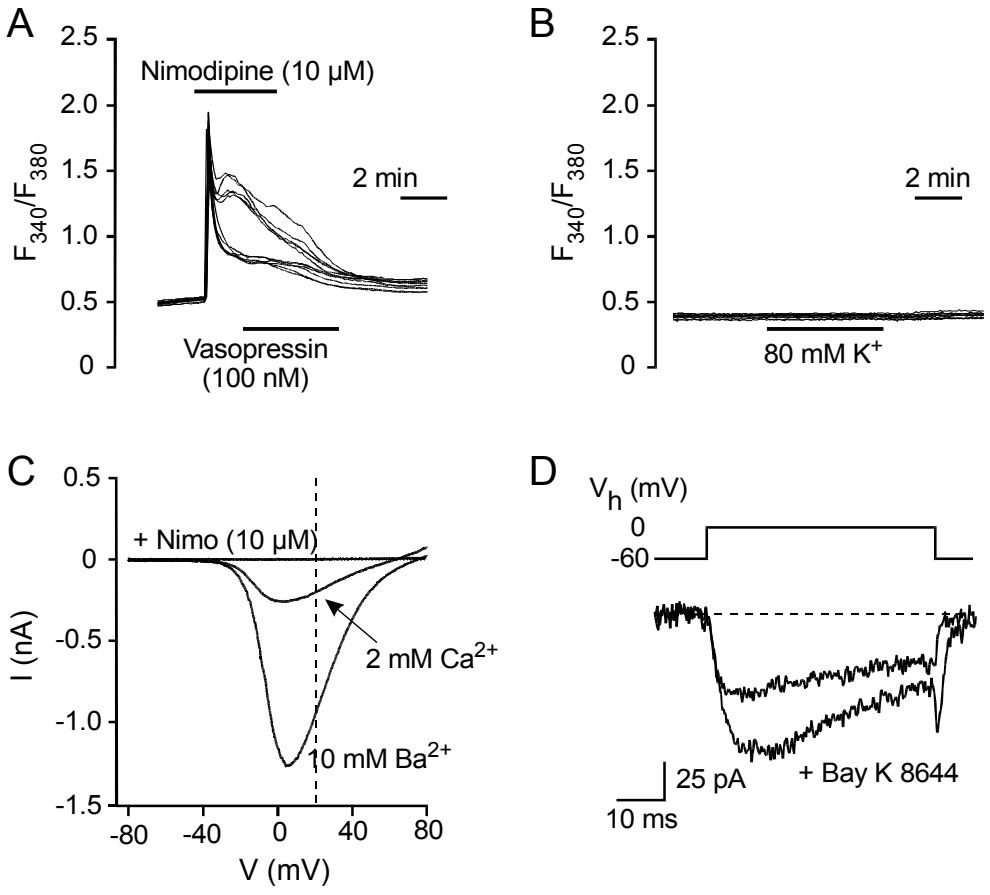

Fig. 8: **Voltage-gated Ca^{2+} channels in A7r5 cells.** *A*: Effect of nimodipine (10 µM), a selective inhibitor of L-type voltage-gated Ca^{2+} channels, on AVP-induced $[Ca^{2+}]_i$ increases in A7r5 smooth muscle cells. *B*: Effect of membrane depolarization elicited by increasing the extracellular K^+ concentration to 80 mM. *C*: Leak-corrected current-voltage relation of voltage-gated Ca^{2+} currents recorded from resting A7r5 cells in physiological solutions (2 mM Ca^2), in solutions where Ca^{2+} was replaced by 10 mM Ba^{2+}, and in the presence of nimodipine (10 µM). The curves were obtained during voltage-ramps from –100 mV to +100 mV. *D*: Ionic current measured during a step depolarization from the holding potential (–60 mV) to 0 mV in a solution containing 2 mM Ca^{2+}. Effect of Bay K8466 (10 µM), a dihydropyridine agonist of L-type voltage-gated Ca^{2+} channels, on the current.

To block currents mediated by voltage-gated K^+ channels, pipette and bath solutions contained Cs^+ instead of K^+. In patch clamp experiments, virtually all of the cells tested showed a voltage-activated inward current with a typical U-shaped *I-V* relation, an apparent activation threshold at around -30 mV and peak currents around +10 mV, indicative of high-voltage-activated Ca^{2+} channels (Fig. 8*C*). Current amplitudes were potentiated by exchanging 2 mM Ca^{2+} for 10 mM Ba^{2+} (Fig. 8*C*). With both Ca^{2+} or Ba^{2+} as charge carrier, the currents were completely inhibited by dihydropyridines such as e.g. nimodipine (10 µM, Fig. 8*C*). Furthermore, the dihydropyridine activator of L-type voltage-gated Ca^{2+} channels Bay K8644 (10 µM) induced an increase in the amplitude of the current elicited by a voltage step from a holding potential of -60 mV to 0 mV (Fig. 8*D*).

Hence, L-type voltage-gated Ca^{2+} channels are present in A7r5 smooth muscle cells, but they do not appear to contribute to AVP-induced Ca^{2+} signalling (see above).

Cation currents activated by vasopressin

Whole-cell voltage-clamp recordings were performed to study AVP-stimulated cationic currents underlying the observed Ca^{2+} signals. To block currents mediated by K^+ channels pipette and bath solutions contained Cs^+, rather than K^+, and voltage-gated Ca^{2+} channels were inhibited by addition of nimodipine (10 µM) to all bath solutions. In about 90 % of the cells tested (n = 288), application of AVP resulted in the rapid, transient activation of a noisy inward current at a holding potential of -60 mV (Fig. 9*A*). Current decay was not influenced by removal of the agonist. The *I-V* relations of the AVP-induced current had a characteristic doubly-rectifying form (Fig. 9*B*) similar to those described for various members of the TRPC channel subfamily in heterologous expression systems (Hofmann *et al*., 1999; Okada *et al*., 1999; Kiselyov *et al*., 2000; Schaefer *et al*., 2000; Inoue *et al*., 2001; Schaefer *et al*., 2002; compare also Fig. 9*C,D*). The currents displayed a reversal potential of about 0 mV, indicative of a nonselective cation current. According to the Nernst equation, the reversal potential of chloride (Cl^-) currents under the experimental conditions used was calculated to be ~ -36 mV. Replacement of external Na^+, Cs^+, and Ca^{2+} by the bulky cation $NMDG^+$ almost completely abolished the inward current, whereas outward currents at positive potentials

were either unaffected or slightly increased (Fig. 10*A*,*B*). Conversely, when Cs^+ in the pipette solution was replaced by $NMDG^+$, no outward currents developed in response to AVP application (Fig. 10*C*). To specifically exclude a contribution of Cl^- currents, the effects of two Cl^- channel blockers on AVP-induced whole-cell currents were studied. The Cl^- channel blockers 5-nitro-2-(3-phenylpropylamino)-benzoate (NPPB, 50 µM, $n = 8$, *data not shown*) and niflumic acid (100 µM, $n = 7$) did not block the AVP-induced current (Fig. 10*D*).

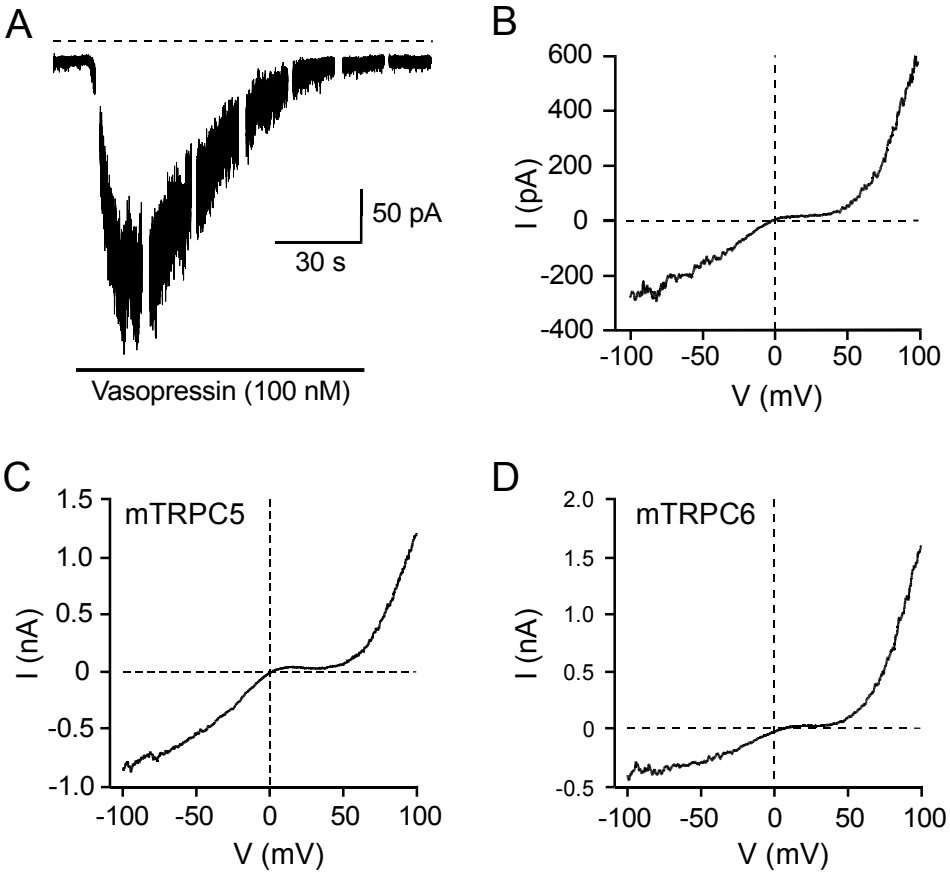

Fig. 9: **Vasopressin-induced whole-cell currents in A7r5 cells and comparison with heterologously-expressed TRPC5 and TRPC6.** *A*: Effect of AVP (100 nM) application on whole-cell currents in A7r5 smooth muscle cells at a holding potential of -60 mV ($[Ca^{2+}]_o = 50$ µM). *B*: Characteristic doubly-rectifying current-voltage relation of the AVP-induced current. The *I-V* relation was obtained during voltage ramps from -100 to +100 mV at the peak of the inward current shown in *A*. For comparison, representative *I-V* relations of agonist-induced currents in mouse TRPC5 (*C*)- and mouse TRPC6 (*D*)-expressing HEK293 cells are shown.

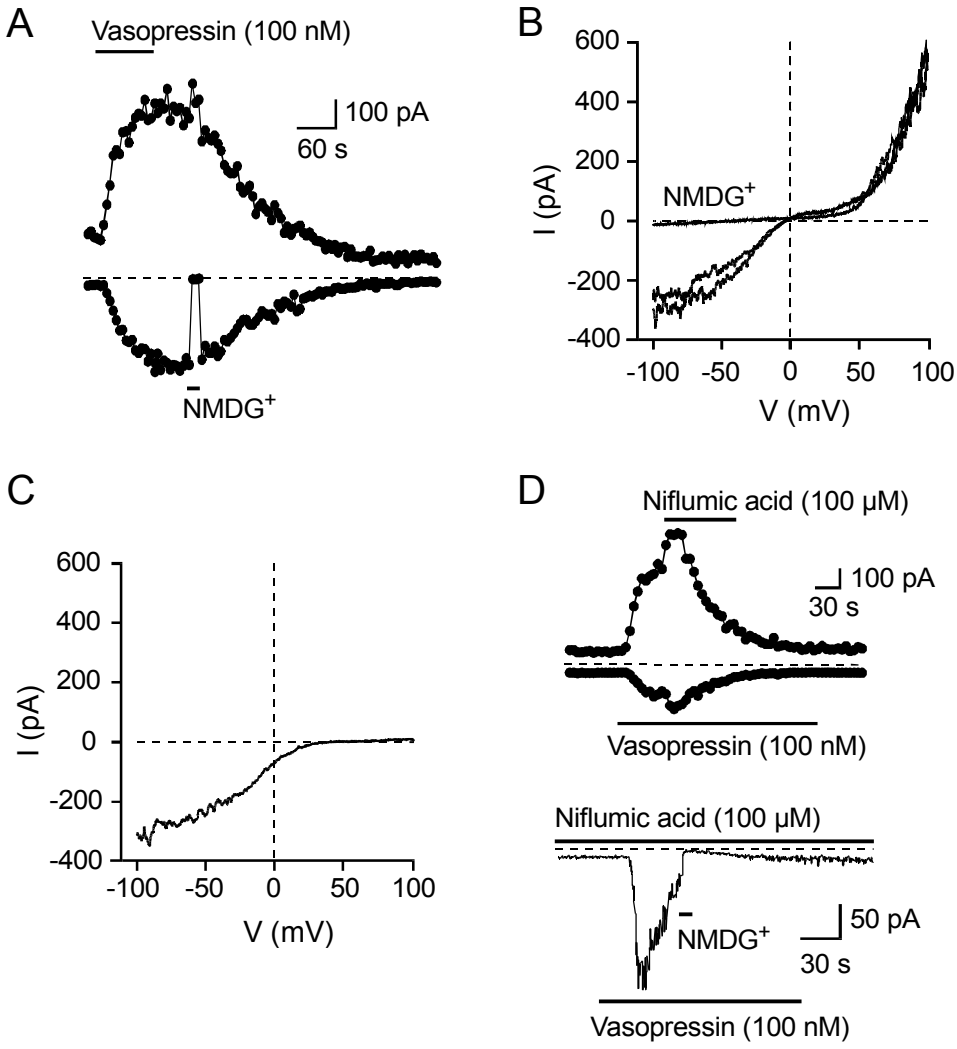

Fig. 10: **Vasopressin-induced whole-cell currents in A7r5 cells are cation currents.** *A*: AVP-induced whole-cell currents in A7r5 cells at -100 and +100 mV in an external solution containing 200 µM Ca^{2+}. *B*: *I-V* relationship of the AVP-induced current in *A*, obtained during voltage ramps from –100 to +100 mV shortly before or after, and during replacement of external cations by $NMDG^+$. *C*: *I-V* relationship of AVP-induced currents in A7r5 cells obtained with a pipette solution where cations were replaced by $NMDG^+$. *D*: Effects of acute application (*upper trace*) of or pretreatment (*lower trace*) with the nonspecific Cl^- channel blocker niflumic acid on AVP-induced currents in A7r5 cells. Whole-cell currents were recorded at -60 mV (*lower trace*) and at -100 or +100 mV (*upper traces*).

Taken together, these results suggest that the AVP-induced current observed in A7r5 cells is a cation current. Since the *I-V* relationship of the AVP-induced current is markedly different from those described for agonist-evoked cation currents in previous studies on A7r5 cells (Van Renterghem *et al*., 1988; Krautwurst *et al*., 1994; Iwasawa *et al*., 1997; Iwamuro *et al*., 1998), the electrophysiological properties of the AVP-induced current were characterized in more detail. In order to relate the results to the possible

involvement of TRPC isoforms, the main interest was focused on the dependence of the endogenous current on $[Ca^{2+}]_o$, on current inhibition and on the activation mechanism.

Dependence of cation currents on $[Ca^{2+}]_o$

The experiments shown above were performed in reduced $[Ca^{2+}]_o$ (50 or 200 µM) because larger response amplitudes were obtained in these solutions. As also reported for noradrenaline-evoked currents in rabbit portal vein smooth muscle cells (Helliwell & Large, 1997), the amplitudes of the AVP-induced currents in A7r5 cells were highly variable and displayed a complex dependence on the external Ca^{2+} concentration. Fig. 11A shows a typical experiment where the AVP-induced current was first evoked in an external solution containing 2 mM Ca^{2+}. After the inward current at -60 mV had reached its peak, $[Ca^{2+}]_o$ was decreased to 50 µM. This decrease in $[Ca^{2+}]_o$ resulted in a substantial increase in current amplitude. Upon readdition of 2 mM Ca^{2+} to the extracellular solution, the current amplitude decreased. These data suggest that Ca_o^{2+} inhibits the AVP-induced cation current. The inhibitory effect of Ca_o^{2+} was observed both at negative and positive potentials (Fig. 11B).

Adding to the complexity of the Ca_o^{2+}-dependence of the AVP-induced current, is the fact that when $[Ca^{2+}]_o$ was further decreased (nominally Ca^{2+}-free solutions or substituting EGTA for external Ca^{2+}) inward current amplitudes did not further increase, but were slightly decreased (n = 5, Fig. 11C, current activation by infusion of AlF_4^- was used, see below), whereas outward currents remained unaffected or increased slightly. Thus, despite its inhibitory actions, Ca_o^{2+} also facilitates AVP-induced cation currents. A statistical analysis of this dual dependence on $[Ca^{2+}]_o$ is presented in Fig. 12A,B.

As shown in Fig. 9, the AVP-induced current in A7r5 cells showed marked rectification and the potentiating effect of Ca^{2+} might be due to the alteration of those rectifying properties. Consequently, current-voltage relationships obtained in high and low Ca_o^{2+} were normalized to the peak current at negative potentials (which is -1) and the resulting normalized I-V curves superimposed (Fig. 11D). The I-V relationships were similar in solutions containing high and low external Ca^{2+}, and the reversal potential of the current remained largely unchanged suggesting that Ca_o^{2+} does not influence current rectification.

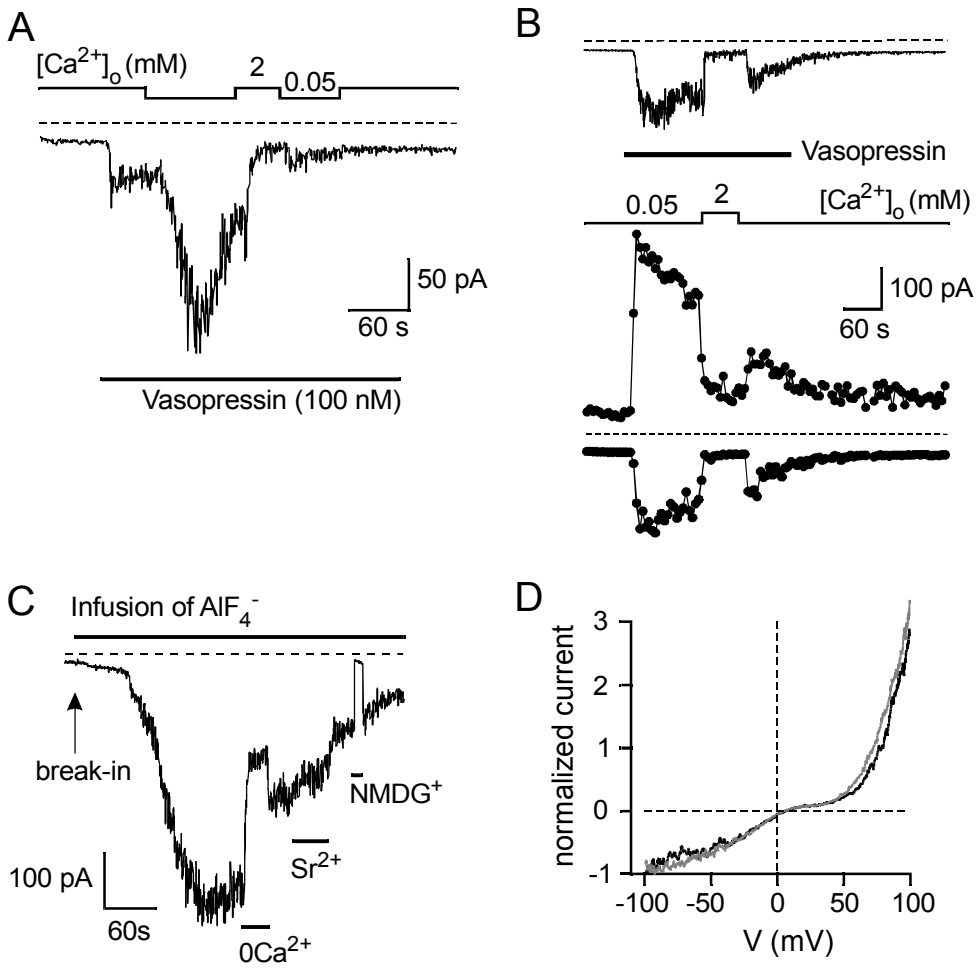

Fig. 11: **Effects of different $[Ca^{2+}]_o$ and external Sr^{2+} on cation currents in A7r5 cells.** *A,B*: Effects of decreasing (*A*) or increasing (*B*) $[Ca^{2+}]_o$ on the amplitude of the AVP-induced currents. Whole-cell currents recorded at -60 mV (*A*, *B upper trace*) and at -100 or +100 mV (*B lower traces*) are shown. *C*: Inward current elicited by infusion of AlF_4^- at -60 mV in an external solution containing 200 µM Ca^{2+}. Effects of Ca^{2+} removal or replacement of Ca^{2+} by Sr^{2+} (2 mM) on the AlF_4^--induced current. *D*: Normalized *I-V* relations of vasopressin-induced currents in external solutions with no (*black trace*) or 2 mM (*grey trace*) Ca^{2+} added. The curves, obtained during voltage-ramps from -100 mV to +100 mV were normalized to the respective maximum inward current.

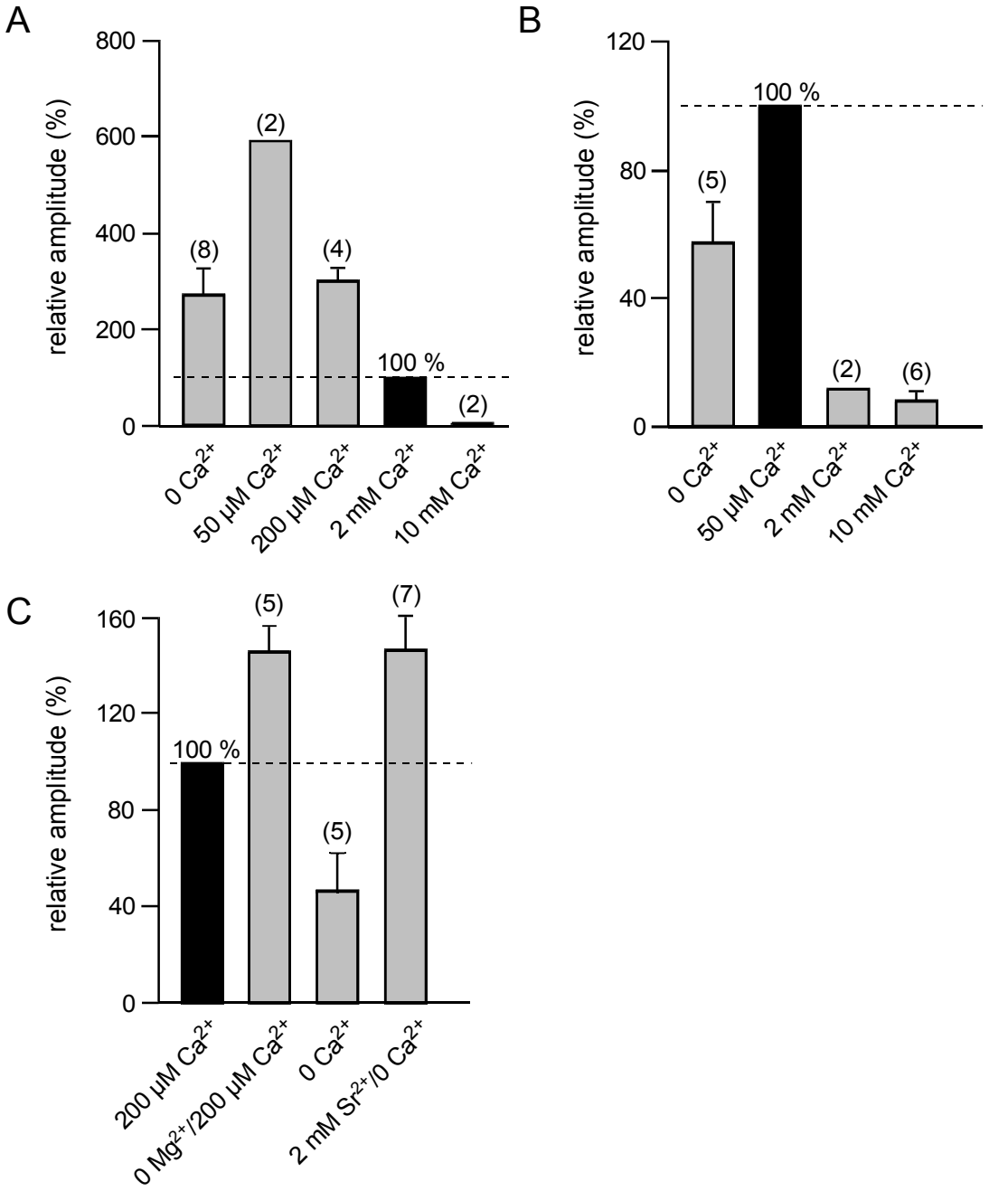

Fig. 12: **Statistical analysis of the effects of external Ca^{2+}, Mg^{2+} and Sr^{2+} on cation currents in A7r5 cells.** *A*: Statistical analysis of the effects of $[Ca^{2+}]_o$ reduction or increase on the amplitude of AVP-induced cation currents recorded at a holding potential of –60 mV. Currents were initially elicited in a bath solution containing 2 mM Ca^{2+}, and the amplitudes obtained during subsequent solution exchanges were normalized to the amplitude determined in 2 mM Ca_o^{2+} (= 100 %). *B*: Same as in *A*, with the exception that the currents were initially elicited in a bath solution containing 50 µM Ca_o^{2+}. Current amplitudes obtained in 50 µM Ca^{2+} were set to 100 %. *C*: Statistical analysis of the effects of Mg^{2+} and Ca^{2+} removal on AVP-induced whole-cell currents at a holding potential of -60 mV. The effects of Ca^{2+} removal were reversed by addition of 2 mM Sr^{2+}. The extracellular solution initially contained 200 µM Ca^{2+}, and relative current amplitudes were obtained by normalizing to the value obtained in 200 µM Ca^{2+} (= 100 %).

Because current amplitudes were larger in extracellular solutions with lower $[Ca^{2+}]_o$, solutions containing 200 µM or 50 µM Ca^{2+} were used for the remainder of the study. In general, cells were less stable in 50 µM $[Ca^{2+}]_o$. At -60 mV, the mean peak inward current densities in response to AVP were 2.3 ± 0.2 pA/pF ($C_m = 61.8 \pm 1.1$ pF, $n = 151$) in 200 µM Ca_o^{2+} and 0.6 ± 0.1 pA/pF ($C_m = 68.8 \pm 2.7$ pF, $n = 44$) in 2 mM Ca_o^{2+}.

Attempts were made to determine the relative permeabilities of the AVP-activated channel for mono- and divalent cations. However, owing to the inhibitory effect of high $[Ca^{2+}]_o$, inward currents in solutions with Ca^{2+} as the only permeant cation were very small and effects of high $[Ca^{2+}]_o$ on baseline ('leak') currents could not be reliably separated from those on the AVP-induced current. This problem was not solved by increasing $[Ca^{2+}]_o$ from 10 to 100 mM. Therefore, the relative Ca^{2+} permeability could not be determined. Likewise, inward currents in extracellular solutions containing only Ba^{2+} or Sr^{2+} as permeant ions, were too small to accurately determine the reversal potential.

Effects of di- and trivalent cations and SKF 96365 on AVP-induced currents

The effects of other di- and trivalent cations, commonly used to block nonselective cation currents, were also studied on AVP-induced currents in A7r5 cells. As can be seen in Fig. 13A,B and Fig. 14, Gd^{3+} (100 µM, n = 4) completely blocked the AVP-induced current at all potentials. A lower concentration of 1 µM was only partially inhibitory (about 40 % inhibition at –100 mV, n = 4; data not shown). Likewise, La^{3+} (100 µM) inhibited AVP-induced inward currents by 100 % (n = 6, Fig. 14). The effects of both La^{3+} and Gd^{3+} at a concentration of 100 µM were not readily reversible.

The divalent cations Ni^{2+} (1 mM, $n = 5$), Co^{2+} (100 µM ($n = 1$), 500 µM ($n = 2$) or 2 mM ($n = 2$); ~ 30 %, ~ 50 % and ~ 90 % inhibition at -100 mV) and Mn^{2+} (2 mM, $n = 5$) only partially blocked AVP-induced inward currents in A7r5 cells (Fig. 13*C* and Fig. 14). Inhibition of AVP-induced currents was readily reversible upon removal of these cations from the bath solution. Outward currents were inhibited to a lesser extent than the inward currents, suggesting a voltage-dependent block by these cations (Fig. 14). By contrast, Ba^{2+} (2 mM, $n = 5$, Fig. 14) only slightly reduced AVP-induced

inward currents and was without effect on outward currents. Sr^{2+} (500 µM or 2 mM, $n = 4$, Fig. 13*C* and Fig. 14) did not change current amplitudes when added to the extracellular solution. Furthermore, Sr^{2+} (2 mM, $n = 8$, Fig. 11*C*, 12*C*) was able to prevent or even reverse the inhibitory action of complete Ca_o^{2+} removal on AVP-induced inward current.

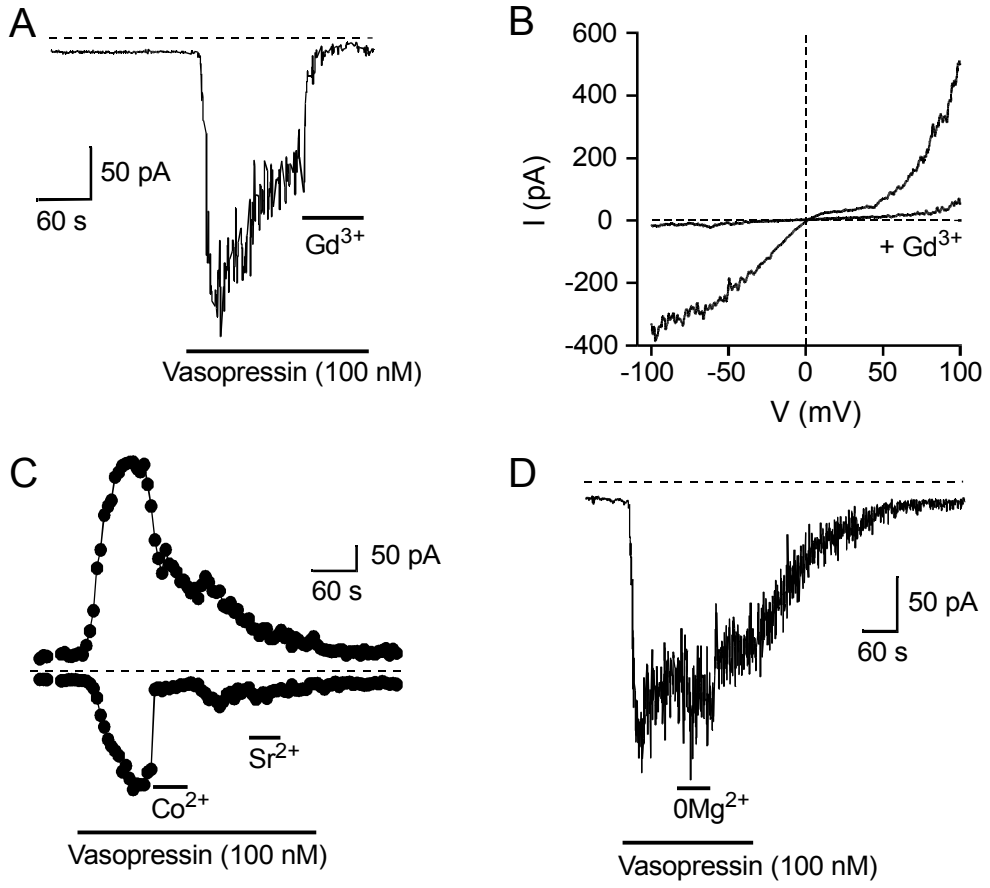

Fig. 13: **Effects of different di- and trivalent cations on vasopressin-induced cation currents in A7r5 cells.** *A*: Whole-cell current at -60 mV in an external solution containing 50 µM Ca^{2+}. Effect of Gd^{3+} (100 µM) application on the AVP-induced current. *B*: *I-V* relationships obtained from the same cell during voltage ramps from -100 to +100 mV before and during addition of Gd^{3+}. *C*: Whole-cell currents at -100 and +100 mV in 200 µM Ca_o^{2+}. Comparison of Co^{2+} (2 mM) and Sr^{2+} (2 mM) effects on the AVP-induced current. *D*: Effects of Mg^{2+} removal on AVP-induced whole-cell currents recorded at -60 mV in an external solution containing 200 µM Ca^{2+}.

Removal of Mg^{2+}, which was normally present at 1 mM in all extracellular solutions, slightly augmented AVP-induced currents ($n = 4$, Fig. 12*C*, 13*D*), while the *I-V* relation remained largely unchanged. SKF 96365 (100 µM), a commonly used organic cation

channel blocker, inhibited AVP-evoked cation currents in A7r5 smooth muscle cells at -60 mV by 98 ± 2 % (n = 5, Fig. 14).

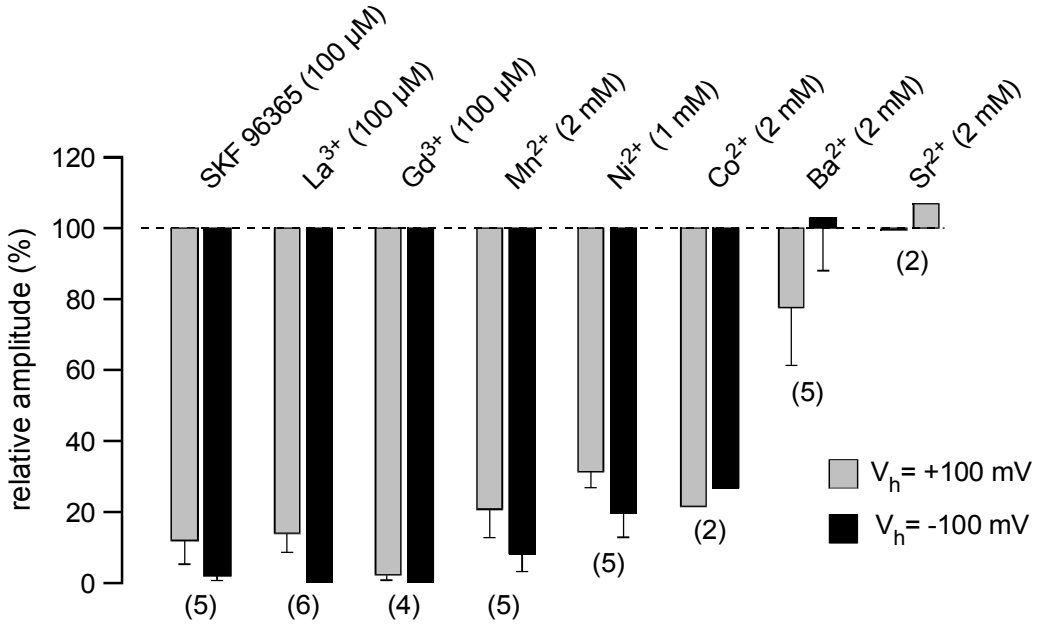

Fig. 14: **Summarized statistical analysis of the effects of di- and trivalent cations and SKF 96365 on vasopressin-induced whole-cell currents in A7r5 smooth muscle cells**. Relative current amplitudes in the presence of the modulators were obtained by normalizing to the value obtained in their absence (= 100 %). $[Ca^{2+}]_o$ was 200 µM in all experiments. The number of experiments is given in parentheses.

Single-channel conductance

For most members of the TRP channel family, single-channel conductances have been estimated from single-channel recordings or fluctuation analysis (Zitt *et al*., 1996; Kiselyov *et al*., 1998; Hofmann *et al*., 1999; Schaefer *et al*., 2000; Yamada *et al*., 2000; Inoue *et al*., 2001; Strübing *et al*., 2001; Schaefer *et al*., 2002). To compare these data with the single-channel properties of the AVP-evoked currents in A7r5 cells, fluctuation analysis was performed. Fluctuation analysis was preferred to single-channel recordings because of the low whole-cell current densities. Whole-cell currents at -60 mV were recorded at increased sampling rates (see Materials & Methods) and leak-subtracted. Mean currents and current variances were calculated for 100-ms periods during the rising phase of the AVP-induced current response. The results of a representative experiment are shown in Fig. 15.

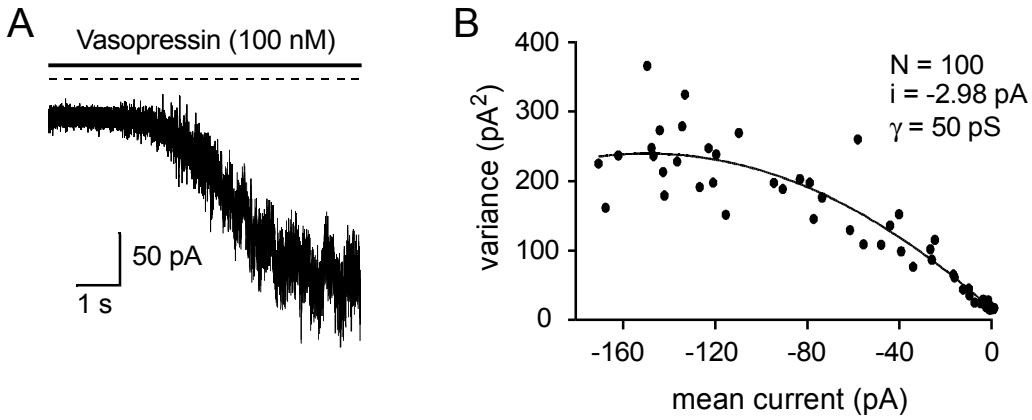

Fig. 15: **Fluctuation analysis of the vasopressin-induced cation current in A7r5 cells.** *A*: Whole-cell current recorded at -60 mV in an external solution containing 200 µM Ca^{2+}. The current was recorded at a sampling rate of 10 kHz (filter frequency: 5 kHz). *B*: Relationship between current variance (σ^2) and mean current (I) as calculated from the current in *A*.

In many cases, the relationship between current variance and mean current was not parabolic but essentially linear, probably because the open probability of the channels was low even at the peak of the current evoked by AVP. Therefore, no reliable estimates of the average number of AVP-activated cation channels present in the plasma membrane of A7r5 cells could be obtained as would have been expected from the equation $\sigma^2 = iI\text{-}I^2/N$ used to fit the plots. In 200 µM Ca_o^{2+}, the mean single-channel current at a holding potential of -60 mV was -1.82 ± 0.13 pA (n = 12). From this a single-channel chord conductance of 30 pS was calculated.

Mechanism of current activation

The mechanism of cation current activation in A7r5 smooth muscle cells was investigated in more detail. Agonists such as 5-hydroxytryptamine (5-HT, 50 µM, n = 8/9, Fig. 16*B*) and endothelin I (100 nM, n = 3/6, *data not shown*), that bind to G protein-coupled receptors and subsequently activate PLCβ, as well as platelet-derived growth factor (PDGF, 40 - 80 ng/ml, n = 5/9, Fig. 16*A*), which activates PLCγ through stimulation of a receptor tyrosin kinase, stimulated a cation current with the typical doubly-rectifying *I-V* relationship in A7r5 cells. In the case of PDGF, current activation was slower than that with agonists that bind to G protein-coupled receptors.

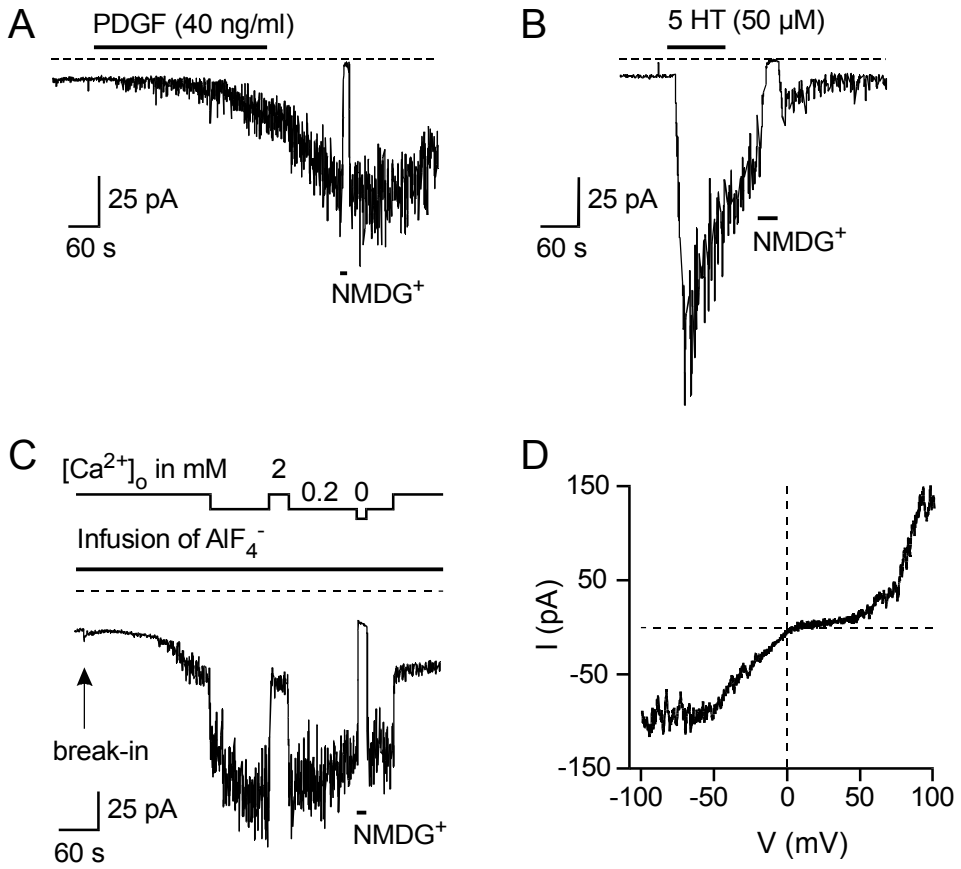

Fig. 16: **Cation currents in A7r5 cells can be activated by stimulation of G protein-coupled receptors and receptor tyrosine kinases, or by direct stimulation of G proteins.** Whole-cell currents recorded at a holding potential of -60 mV in an external solution containing 50 µM (*B*) or 200 µM (*A*) Ca_o^{2+}. Inward currents were evoked by application of platelet-derived growth factor (*A*, 40 ng/ml) and 5-hydroxytryptamine (*B*, 50 µM). *C*: Infusion of AlF_4^- elicted an inward current at –60 mV with a doubly-rectifying current-voltage relation (*D*, leak-subtracted). Effects of decreases and increases in $[Ca^{2+}]_o$, and of replacement of external cations by $NMDG^+$ on AlF_4^--induced currents are shown.

The above data suggest a role for PLC in current activation as described for other members of the TRP channel family (Hofmann *et al*., 1999; Okada *et al*., 1999; McKay *et al*., 2000; Schaefer *et al*., 2000; Strübing *et al*., 2001; Schaefer *et al*., 2002).

To determine whether direct activation of heterotrimeric G proteins can stimulate the cation current in A7r5 cells, aluminium fluoride (AlF_4^-, Sternweis & Gilman, 1982; Bigay *et al*., 1985; Bigay *et al*., 1987; Kahn, 1991) was added to the intracellular solution. In A7r5 cells, infusion of AlF_4^- activated a cation current with variable delay (n = 20/23, Fig. 16*C*). The current displayed a doubly-rectifying current-voltage relation (Fig. 16*D*) identical to that described for AVP-induced currents. Consistent with the currents evoked by AVP, the amplitude of the AlF_4^--evoked current was

increased by decreasing $[Ca^{2+}]_o$, and inward current was abolished by removal of extracellular cations (Fig. 16*C*).

To test for a role of intracellular store depletion in the activation of AVP-induced cation currents in A7r5 cells, protocols were used that have previously been shown to activate store-operated channels in other preparations (Fasolato & Nilius, 1998). Infusion of $InsP_3$ (100 μM) in a Ca^{2+}-free 10 mM EGTA pipette solution did not change the holding current (n = 9). Similarly, no current activation could be obtained in solutions containing 100 nM free Ca^{2+} buffered with 10 mM EGTA (n = 12, Fig. 17*A*). However, after 5 min of $InsP_3$ infusion, 10 of the 19 cells tested responded to AVP with activation of cation currents. As caffeine (5 mM) application did not result in a measurable Ca^{2+} increase in fura-2-based Ca^{2+}-imaging experiments (n = 0/33, *data not shown*), ryanodine receptors do not seem to contribute significantly to Ca^{2+} signalling in A7r5 cells and hence, depletion of intracellular stores by $InsP_3$ can be expected to be complete (also see Byron & Taylor, 1993). Likewise, passive depletion of internal Ca^{2+} stores by addition of the SERCA Ca^{2+}-ATPase inhibitor thapsigargin (10 μM, n = 3) did not result in activation of a cation current in A7r5 cells (*data not shown*). Current activation was not impaired by infusion of the $InsP_3$ receptor agonist heparin (5 mg/ml) for 5 min prior to AVP application (n = 4, Fig. 17*B*). Infusion of cells with high Ca^{2+} (10 μM) revealed that the cation conductance in A7r5 cells was not Ca^{2+}-activated (n = 7, Fig. 17*C*). In four cells, AVP was able to induce current activation after 5 min of 10 μM Ca^{2+} infusion.

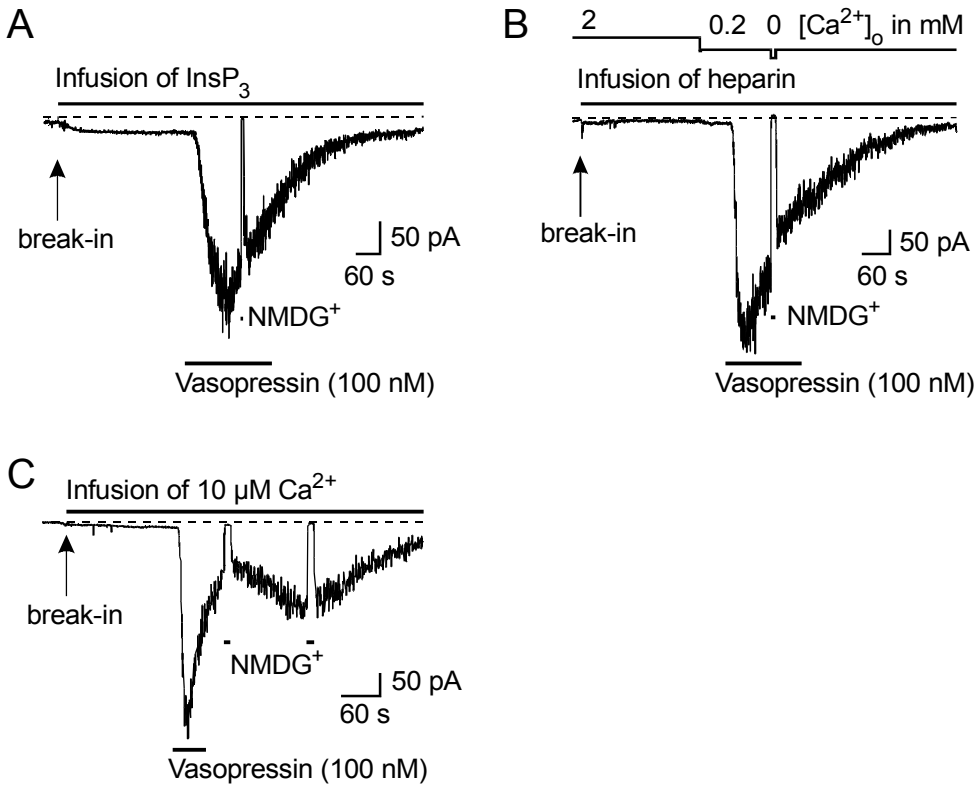

Fig. 17: **Cation currents in A7r5 cells are not activated by store depletion or $[Ca^{2+}]_i$ increases.** *A*-*C*: Whole-cell currents recorded at –60 mV in 200 µM Ca_o^{2+}. *A*: In contrast to AVP (100 nM) application, infusion of $InsP_3$ (100 µM) did not evoke currents in A7r5 smooth muscle cells. *B*: Inhibition of Ca^{2+} release from internal stores by infusion of the $InsP_3$ receptor blocker heparin (5 mg/ml), did not prevent AVP-induced current activation. *C:* Infusion of 10 µM Ca^{2+} did not activate currents, nor did it prevent current activation by subsequent addition of AVP.

The TRPC3/6/7 subfamily of TRP channels was shown to be activated by diacylglycerols independently of PKC stimulation (Hofmann *et al*., 1999; Okada *et al*., 1999; McKay *et al*., 2000) whereas TRPC4/5 are unresponsive to the lipids (Hofmann *et al*., 1999; Schaefer *et al*., 2000). To assess the role of DAG in cation current activation in A7r5 cells, the membrane-permeable DAG analogue 1-oleoyl-2-acetyl-*sn*-glycerol (OAG) was added to the extracellular solution during whole-cell recordings. As shown in Fig. 18*A*, OAG evoked cation currents ($n = 45/53$) with properties identical to the AVP-induced current (Fig. 18*B*). Comparison of the amplitudes of the current responses elicited by different OAG concentrations indicated that responses close to maximum were obtained at a concentration of 100 µM. Responses evoked by 10 µM OAG only reached 30 ± 3 % ($n = 4$) of the amplitudes observed upon subsequent application of 100 µM OAG (*data not shown*). Raising the OAG

concentration from 100 µM to 500 µM, resulted in no further increase (n = 6/8) or a slight increase (n = 2/8) in response amplitude (*data not shown*). As OAG concentrations above 100 µM rendered recordings increasingly unstable, 100 µM OAG was routinely used.

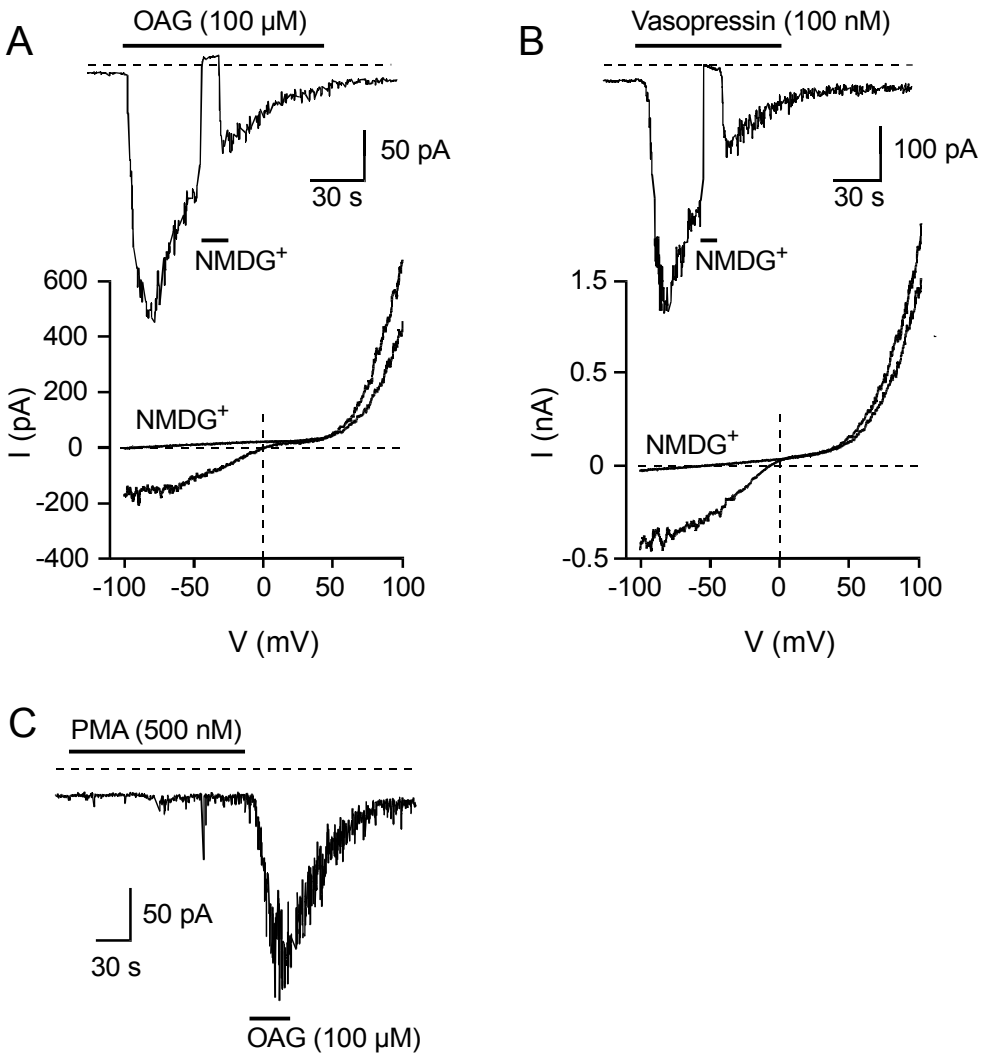

Fig. 18: **Cation currents in A7r5 cells are activated by diacylglycerols independently of protein kinase C.** *A*,*B*: Comparison of the effects of the membrane-permeable diacylglycerol analogue OAG (100 µM) and AVP (100 nM) on currents in A7r5 cells. Whole-cell currents recorded at -60 mV in 200 µM Ca_o^{2+} (*upper panels*) and corresponding *I-V* relations (*lower panels*). Effects of replacement of external cations by $NMDG^+$ are shown. *C*: Effects of the protein kinase C (PKC) activator phorbol-12-myristate-13-acetate (PMA) on whole-cell currents recorded at -60 mV. As a control, OAG (100 µM) was added subsequently.

To test for an involvement of PKC in the OAG-induced current response, the effects of the PKC activator phorbol-12-myristoyl-13-acetate (PMA, 500 nM) on whole-cell currents in A7r5 cells were studied (Fig. 18*C*). Acute application of PMA did not elicit

any current in A7r5 cells ($n = 4$) whereas subsequent application of OAG induced the typical cation current ($n = 2/4$), though its amplitude was reduced. Likewise, in fura-2 experiments, preincubation with PMA (500 nM) for several minutes reduced the response amplitudes to subsequent application of AVP ($n = 59$, *data not shown*). However, again, PMA itself did not increase $[Ca^{2+}]_i$ in A7r5 cells ($n = 59$, *data not shown*). Hence, activation of PKC, rather than activating Ca^{2+} influx, inhibits AVP-induced Ca^{2+} entry. It can, thus, be concluded that current activation by OAG is independent of PKC.

Like for AVP-induced currents, the amplitudes of the currents activated by 100 µM OAG were highly variable, ranging from 0.1 pA/pF to 8.9 pA/pF at -60 mV in 200 µM Ca_o^{2+}. The mean peak current density in response to 100 µM OAG was 1.4 ± 0.3 pA/pF ($n = 36$), a value smaller than, but not statistically significant from that for AVP-induced currents under identical conditions.

To investigate whether the OAG-stimulated current accounts for all or only part of the AVP-induced current increase, OAG-induced currents were recorded before and after addition of AVP, and vice versa. In both cases, the second substance was applied after the response to the first substance had reached its peak. When OAG was applied after AVP, some cells showed no additional effect upon OAG application ($n = 5/11$, Fig. 19*A*, *left trace*), others displayed a small increase in current ($n = 4/11$, Fig. 19*A*, *middle trace*), and two cells exhibited a substantial increase in current amplitude which well exceeded the peak response to the preceding AVP application (Fig. 19*A*, *right trace*). When AVP was applied after OAG, three out of seven cells showed no further increase in current upon AVP application (Fig. 19*B*, *right trace*). The remaining four cells showed a very small increase in current amplitude which did not exceed the peak response to the preceding OAG application (Fig. 19*B*, *left trace*). Hence, OAG- and AVP-induced currents did not appear to be additive.

Taken together, these data support a contribution of the TRPC3/6/7 subfamily of TRP channels to cation currents in A7r5 smooth muscle cells.

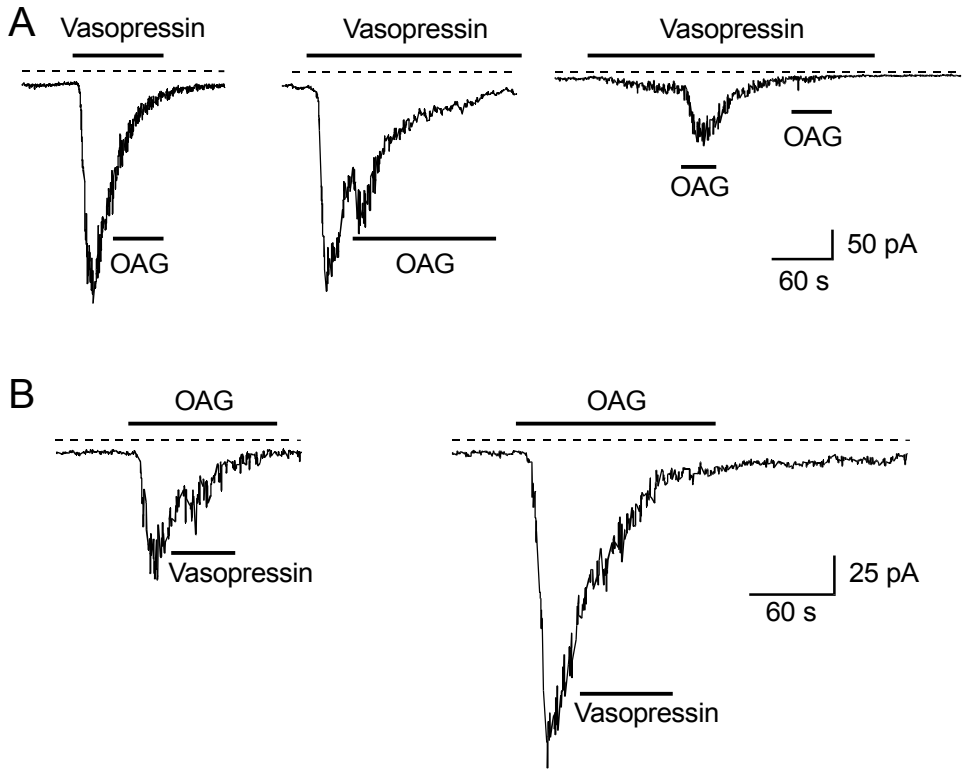

Fig. 19: **Vasopressin and OAG effects are not additive**. *A*: Effects of acute OAG (100 µM) application on AVP (100 nM)-induced whole-cell currents in A7r5 cells recorded at -60 mV. *B*: Effects of acute AVP (100 nM) application on OAG (100 µM)-induced whole-cell currents in A7r5 cells recorded at -60 mV.

Ca^{2+} entry in A7r5 cells has been reported to be activated by arachidonic acid (Broad *et al*., 1999) and arachidonic acid, like several other polyunsaturated fatty acids, has been shown to activate Drosophila TRP and TRPL (Chyb *et al*., 1999). Therefore, arachidonic acid (AA, 100 µM (n = 8), 50 µM (n = 5), 20 µM (n = 2), 10 µM (n = 8)) was tested for its ability to induce currents in A7r5 cells (*data not shown*). Experiments were complicated by the fact that AA rendered recordings unstable, leading to loss of the cell between 10 s and 4 min after application. AA did not activate a cation current with a doubly-rectifying *I-V* relation in any of the cells tested.

Effect of flufenamate on cation currents

Flufenamate (FFA), which blocks many types of cation channels (see e.g. Chen *et al*., 1993; Popp *et al*., 1993), has been shown to reversibly enhance currents mediated by mTRPC6, whereas currents mediated by mTRPC3 and mTRPC7 were inhibited by the drug (Inoue *et al*., 2001). Thus, FFA is a pharmacological tool that may help to clarify

which members of the TRPC3/6/7 group are involved in agonist-induced cation currents in A7r5 cells. FFA (100 µM) increased cation currents induced by infusion of AlF_4^- (*n* = 7, Fig. 20*A*), by application of OAG (*n* = 10/13, Fig. 20*B*) or AVP (*n* = 4/5, *data not shown*). The remaining cells did not show any change in current levels upon application of FFA. Similar stimulatory effects to those of flufenamate on AVP-induced currents were observed with niflumic acid (100 µM, *n* = 3/4).

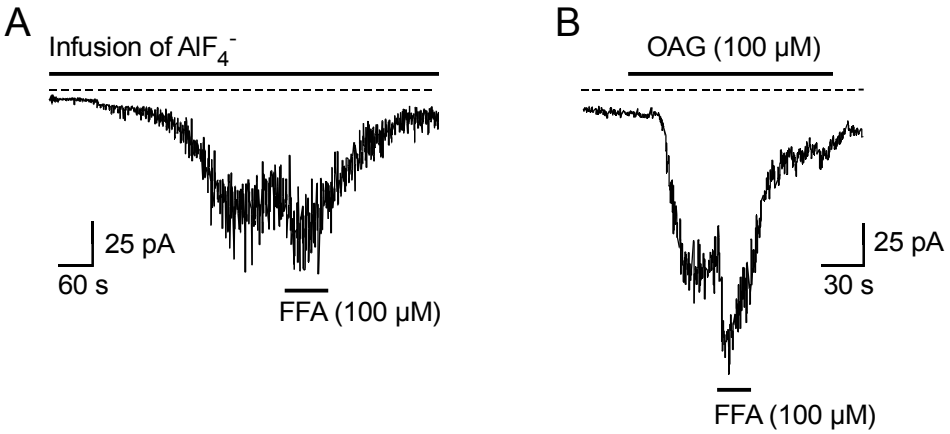

Fig. 20: **Flufenamate increases cation currents in A7r5 cells.** *A*,*B*: Whole-cell currents at -60 mV in 200 µM Ca_o^{2+}. Effects of addition of flufenamate (FFA, 100 µM) on currents elicited by infusion of AlF_4^- (*A*) or application of OAG (100 µM, *B*).

Northern hybridization analysis

The biophysical and pharmacological data obtained from electrophysiological experiments suggest an involvement of TRPC6 in agonist-induced nonselective cation currents in A7r5 smooth muscle cells. In order to substantiate this conclusion, a more direct approach was taken by identifying the TRPC channels expressed in A7r5 cells. Since antibodies are not commercially available for all mammalian members of the TRPC subfamily, the expression of mRNA for TRPC1 - 7 was studied. By Northern hybridization analysis, TRPC6 mRNA was found to be abundantly expressed in A7r5 smooth muscle cells (Fig. 21). Transcripts for TRPC2, -3, -4, -5 and -7 could not be detected in these cells although prominent signals were present in the controls (Fig. 21). By contrast, expression of TRPC1 mRNA was also detectable in A7r5 cells (Fig. 21). Detection of TRPC1 was only possible after purification of mRNA from the total RNA used for all other experiments. When total RNA was used only blurred signals were obtained in A7r5 cells and in controls (*data not shown*). Using purified mRNA, distinct

bands were observed in brain and A7r5 cells (Fig. 21). Northern hybridization experiments were repeated at least twice for each member of the TRPC subfamily, using different RNA preparations.

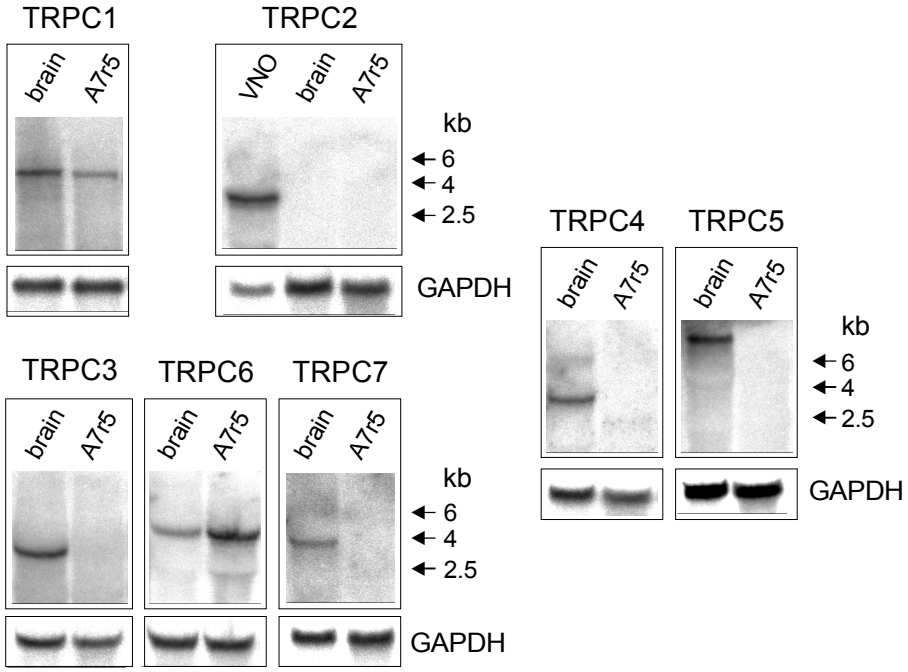

Fig. 21: **mRNAs of TRPC1 and TRPC6 are present in A7r5 cells.** Autoradio-graphs of northern blots hybridized with cDNA probes specific for rat TRPC1 – 7. RNA isolated from rat brain served as a positive control, except for TRPC2, where RNA purified from the rat vomeronasal organ was used as a control.

For all autoradiographs, except that for TRPC2 expression, rat brain RNA served as a positive control. In the case of TRPC2 expression analysis, no signal was detected in rat brain and, thus, RNA derived from the rat vomeronasal organ, where abundant expression has been described previously (Liman *et al*., 1999), was used as a positive control.

3.1.2. TRPC channels in other smooth muscle cell preparations

The evidence presented above suggests that TRPC6 is involved in receptor-stimulated nonselective cation currents in A7r5 smooth muscle cells. To investigate whether TRPC6 plays a general role in vasoconstrictor-induced responses in vascular smooth muscle cells, or whether its functions are restricted to certain vessel types or developmental states, preliminary studies using two other smooth muscle cell

preparations were performed. In one set of experiments, the clonal cell line RVF-SMC derived from the rat vena cava was studied. This cell line was established by Franke *et al*. (1979) and found to have retained several important smooth muscle cell features (Franke *et al*., 1980). Moreover, primary cultures of smooth muscle cells derived from neonatal or adult rat aorta provided by Dr. Peter Reusch were used.

3.1.2.1. RVF-SMC cells

Because virtually no information on PLC-dependent Ca^{2+} signalling is available for RVF-SMC cells, different agonists were tested for their ability to induce $[Ca^{2+}]_i$ increases in these cells. Of all agonists tested, AVP (100 nM) was most effective in raising intracellular Ca^{2+} levels (n = 363/363, Fig. 22*A*). In addition, endothelin I (ET I, 100 nM, n = 140/153, Fig. 22*A*) and the thromboxane A_2 mimetic U46619 (10 µM, n = 37/40, Fig. 22*A*) elicited a substantial increase in F_{340}/F_{380} in RVF-SMC (Fig. 22*A*). Interestingly, ET I-induced $[Ca^{2+}]_i$ increases were consistently delayed by more than one minute compared to the responses elicited by the other agonists. ATP-induced $[Ca^{2+}]_i$ increases were comparatively small (n = 32/38, *data not shown*), whereas angiotensin II (1 µM; n = 0/190, *data not shown*) and noradrenaline (100 µM; n = 0/190, Fig. 22*A*) did not elicit any response. Because AVP was most effective in increasing $[Ca^{2+}]_i$ in RVF-SMC, it was used in all further experiments.

To decide whether and to what extent L-type voltage-gated Ca^{2+} channels contributed to the AVP-induced $[Ca^{2+}]_i$ increases in RVF-SMC the effects of the blocker nimodipine (10 µM) and the agonist Bay K8644 (10 µM) were studied. As shown in Fig. 22*B*, acute application of nimodipine in the presence of AVP did not reduce the amplitude of the AVP-induced response (*middle trace*, n = 119) and only a negligible increase in the AVP-induced response amplitude was observed when Bay K8644 was added to the bath solution (*right trace*, n = 146). Accordingly, depolarization of RVF-SMC by extracellular solutions containing high concentrations of K^+ (80 mM, n = 40, or 145 mM, n = 112) instead of Na^+ only resulted in very small increases in cytosolic Ca^{2+} levels (Fig. 22*B*, *right trace*). Taken together, these results suggest that the contribution of voltage-gated Ca^{2+} channels to AVP-induced $[Ca^{2+}]_i$ increases in RVF-SMC was negligible as was the case for AVP-induced Ca^{2+} signalling in A7r5 smooth muscle cells.

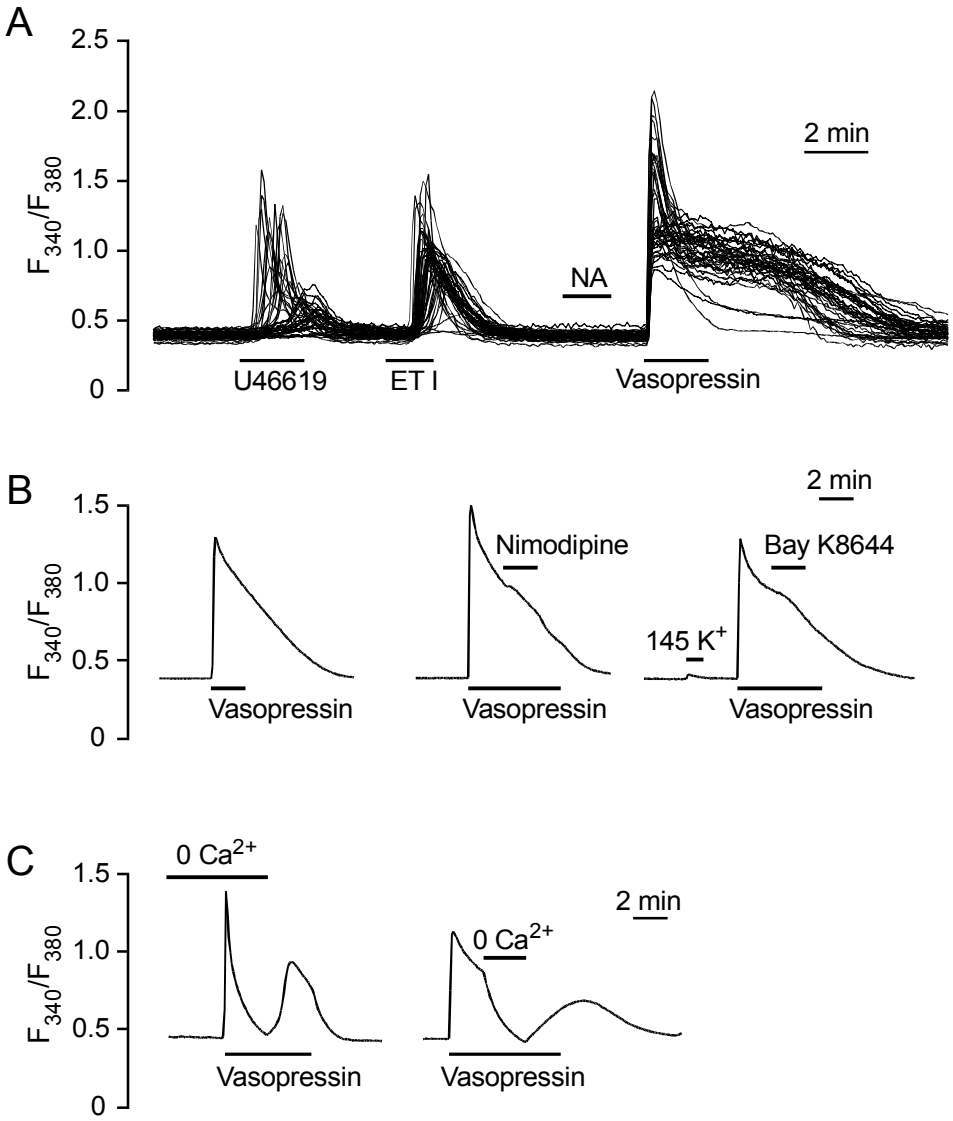

Fig. 22: **Agonist-induced Ca^{2+} signalling in RVF-SMC.** *A*: Time-dependent changes in $[Ca^{2+}]_i$ (revealed by changes in fluorescence ratio F_{340}/F_{380}) of individual, fura-2-loaded RVF-SMC upon application of the thromboxane A_2 mimetic U46619, endothelin I (ET I), noradrenaline (NA), and AVP. *B*: Effects of nimodipine (10 µM, *middle trace*) and Bay K8644 (10 µM, *right trace*) on AVP (100 nM)-induced $[Ca^{2+}]_i$ changes (also see *left trace*, without nimodipine). The traces are the mean of 19, 40 and 32 cells, respectively. *C*: Effects of removal and readdition of Ca_o^{2+} during AVP application. *Left trace*: The AVP-induced response was elicited in the absence of Ca_o^{2+} and Ca_o^{2+} subsequently added. *Right trace*: Acute Ca_o^{2+} removal during the AVP-induced response. The traces are the mean of 39 and 40 cells, respectively.

When AVP was applied to RVF-SMC in the absence of external Ca^{2+}, $[Ca^{2+}]_i$ increases were still observed, but these declined to baseline much faster than in Ca^{2+}-containing bath solution. Readdition of Ca^{2+} led to an increase in F_{340}/F_{380} (n = 95/95, Fig. 22*C*, *left trace*). Likewise, Ca^{2+} removal during prolonged application of AVP resulted in

reversible inhibition of the AVP-induced $[Ca^{2+}]_i$ increases ($n = 99/100$, Fig. 22C, *right trace*). Hence, like in A7r5 cells, AVP stimulated Ca^{2+} influx into RVF-SMC.

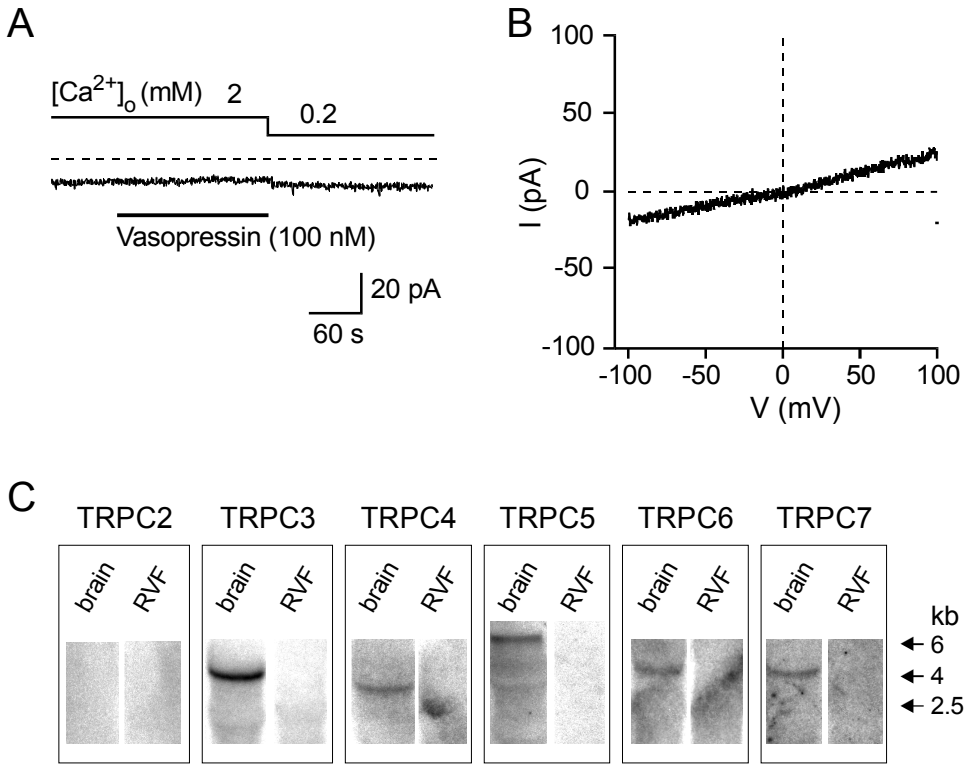

Fig. 23: *A:* **Vasopressin did not induce currents in RVF-SMC cells** Effect of AVP (100 nM) application on whole-cell currents in RVF-SMC at a holding potential of -60 mV. *B*: *I-V* relation of the currents in RVF-SMC in the presence of AVP. The *I-V* relations were obtained during voltage ramps from -100 to +100 mV. *C*: **mRNAs of TRPC2 - 7 are not present in RVF-SMC.** Autoradiographs of northern blots hybridized with cDNA probes specific for rat TRPC2 – 7. RNA isolated from rat brain served as a positive control, except for TRPC2 (positive control for TRPC2: rat vomeronasal organ , cf. Fig. 21).

Whole-cell experiments were performed to examine the currents that underlie the observed AVP-induced Ca^{2+} entry. Like for experiments with A7r5 cells, nimodipine was added to the bath solution to inhibit L-type voltage-gated Ca^{2+} channels and K^+ currents were blocked by exchanging K^+ in pipette and bath solutions for Cs^+. Surprisingly, under these conditions, neither AVP application ($n = 5$, Fig. 23*A*) nor infusion of AlF_4^- ($n = 3$, *data not shown*) resulted in detectable cation currents in RVF-SMC. Only Cl^- currents (negative reversal potential and typical outwardly-rectifying *I-V* relation) developed upon AVP application in some cells ($n = 4/8$). When K^+ instead of Cs^+ was used in all solutions, AVP elicited prominent K^+ currents in RVF-SMC ($n = 4/5$) suggesting that the vasoconstrictor was effective under the conditions used

(*data not shown*). Consistent with the absence of AVP-induced nonselective cation currents in whole-cell recordings, no mRNA for TRPC2-6 was detected by northern hybridization analysis in these cells (Fig. 23*B*).

In conclusion, the above data suggest that in contrast to the results obtained for A7r5 smooth muscle cells, TRPC6 does not seem to play a prominent role in RVF-SMC.

3.1.2.2. Smooth muscle cells derived from neonatal and adult rat aorta

Ratiometric Ca^{2+} imaging with the fluorescent Ca^{2+} indicator fura-2 revealed that smooth muscle cells derived from neonatal or adult rat aorta differ considerably in their responsiveness to different vasoconstrictors. Aortic smooth muscle cells from neonatal rats were found to respond exclusively to AVP (100 nM, $n = 65/71$), whereas ET I (100 nM, $n = 3/71$), noradrenaline (NA, 100 µM, $n = 0/71$), U46619 (10 µM, $n = 0/40$, *data not shown*) and angiotensin II (AT II, 1 µM, $n = 0/31$) were essentially ineffective (Fig. 24*A*, *left trace*). By contrast, aortic smooth muscle cells derived from adult rats (Fig. 24*A*, *right trace*) were virtually unresponsive to AVP (100 nM, $n = 2/38$), but exhibited prominent increases in F_{340}/F_{380} upon application of ET I (100 nM, $n = 34/55$) and noradrenaline (100 µM, $n = 19/30$). Interestingly, in many cases, noradrenaline responses were only evident when the agonist was applied after ET I, but not when noradrenaline was added to previously unstimulated cells. AT II (1 µM, $n = 2/39$, *data not shown*) was barely effective. The divergent agonist profile of aortic smooth muscle cells from neonatal and adult rats demonstrated that different developmental states of vascular smooth muscle cells may display different properties.

Whole-cell recordings were performed using the same recording conditions as for A7r5 cells and RVF-SMC. When AVP was applied to cells from neonatal rats, one out of nine cells responded with a small, noisy current increase at a holding potential of –60 mV. The inward current was blocked when extracellular cations were replaced with $NMDG^+$, indicating that the current was carried by cations. Interestingly, the *I-V* relation was doubly rectifying and indistinguishable from that recorded in A7r5 cells upon AVP stimulation (Fig. 24*B*, *left part*). Accordingly, infusion of AlF_4^- into smooth muscle cells obtained from adult rat aorta resulted in a small, noisy inward current at –60 mV ($n = 3/8$; Fig. 24*B*, *right part*). This current was $NMDG^+$-sensitive and exhibited the typical doubly-rectifying *I-V* relation (Fig. 24*B*, *right part*), indicative of most

TRPC channels. Information on TRPC channel isoforms expressed in aortic smooth muscle cells derived from neonatal or adult rats has not yet been obtained. Future studies will have to clarify whether TRPC6 plays a role in mediating the cation currents in these cells.

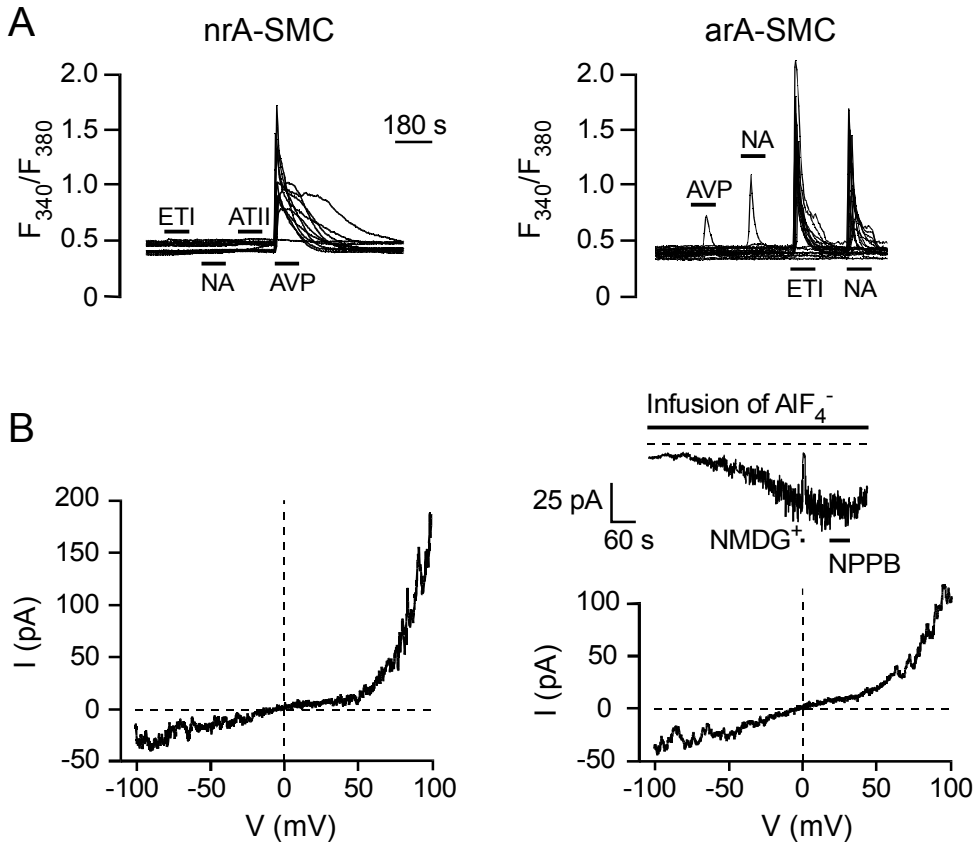

Fig. 24: *A*: **Agonist-induced Ca^{2+} signalling in primary cultures of rat aortic smooth muscle cells.** Time-dependent changes in $[Ca^{2+}]_i$ (revealed by changes in fluorescence ratio F_{340}/F_{380}) of individual, fura-2-loaded smooth muscle cells derived from neonatal (nrA-SMC, *left trace*) or adult (arA-SMC, *right trace*) rats upon application of different agonists (ET I: endothelin I, NA: noradrenaline, AT II: angiotensin II, AVP). *B:* **Cation currents in primary-cultured rat aortic smooth muscle cells.** *I-V* relation of vasopressin-induced currents in smooth muscle cells derived from neonatal rats (*left trace*). AlF_4^--induced whole-cell currents at a holding potential of –60 mV and the corresponding *I-V* relation at the peak of the inward current recorded in cells derived from adult rats (*right traces*). The *I-V* relations were obtained during voltage ramps from -100 to +100 mV.

3.2. Comparison of the biophysical properties of recombinant rat TRPC6 and mouse TRPC5

To compare the properties of the native channel endogenous to A7r5 cells with heterologously-expressed TRPC6, rat TRPC6 was cloned and electrophysiologically characterized in recombinant expression studies. Importantly, rat orthologues of TRPC6 have, to date, only been studied in fluorometric experiments (Zhang & Saffen, 2001) and, thus, no biophysical data are available for these proteins.

TRPC6 belongs to a subgroup of TRPC channels (TRPC3/6/7) that has been reported to be structurally and functionally distinct from another subgroup formed by TRPC4 and TRPC5 (see Introduction). Some of the functional disparities such as regulation by external Ca^{2+} (Okada *et al*., 1998; Okada *et al*., 1999; Schaefer *et al*., 2000; Inoue *et al*., 2001) as well as by the lanthanide ions La^{3+} and Gd^{3+} (Kamouchi *et al*., 1999; Okada *et al*., 1999; Halaszovich *et al*., 2000; Schaefer *et al*., 2000; Strübing *et al*., 2001; Schaefer *et al*., 2002) have not yet been well characterized but are potentially an important distinguishing feature of these groups of channels and, thus, might provide an important tool to aid the identification of their role in native cells.

Therefore, the second part of the present study was devoted to the direct comparison of the functional properties of currents mediated by heterologously-expressed TRPC5 (provided by Dr. Michael Schaefer) and TRPC6 with respect to their regulation by external Ca^{2+} and lanthanide ions.

3.2.1. Cloning and structure of rat TRPC6

TRPC6 was cloned from rat brain and A7r5 cells using an RT-PCR-based strategy. For primer design, recent information available on rat TRPC6 (Zhang & Saffen, 2001) was used. Zhang & Saffen (2001) reported the existence of three different splice variants for rat (r)TRPC6, designated as rTRPC6A, rTRPC6B and rTRPC6C. In contrast to these findings and in accordance with results described for mouse, canine and human TRPC6 (Boulay *et al*., 1997; Hofmann *et al*., 1999; Walker *et al*., 2001), only a single TRPC6 isoform, could be amplified in present study.

A

```
1    MSRGNENRLTHRRQTVLREKGRRLANRGPAYMFNDHSTSLSIEEERFLDAAEYGNIPVVR
61   KMLEECLSLNVNCVDYMGQNALQLAVANEHLEITELLLKKENLSRVGDALLLAISKGYVR
121  IVEAILNHPAFAEGKRLATSPSQSELQQDDFYAYDEDGTRFSHDVTPIILAAHCQEYEIV
181  HTLLRKGARIERPHDYFCKCTECSQKQKHDSFSHSRSRINAYKGLASPAYLSLSSEDPVM
241  TALELSNELAVLANIEKEFKNDYRKLSMQCKDFVVGLLDLCRNTEEVEAILNGDAETRQP
301  GDLARPNLSRLKLAIKYEVKKFVAHPNCQQQLLSIWYENLSGLRQQTMAVKFLVVLAVAI
361  GLPFLALIYWCAPCSKMGKILRGPFMKFVAHAASFTIFLGLLVMNAADRFEGTKLLPNET
421  STDNARQLFRMKTSCFSWMEMLIISWVIGMIWAECKEIWTQGPKEYLFELWNMLDFGMLA
481  IFAASFIARFMAFWHASKAQSIIDANDTLKDLTKVTLGDNVKYYNLARIKWDPTDPQIIS
541  EGLYAIAVVLSFSRIAYILPANESFGPLQISLGRTVKDIFKFMVIFIMVFVAFMIGMFNL
601  YSYYIGAKQNEAFTTVEESFKTLFWAIFGLSEVKSVVINYNHKFIENIGYVLYGVYNVTM
661  VIVLLNMLIAMINSSFQEIEDDADVEWKFARAKLWFSYFEEGRTLPVPFNLVPSPKSLLY
721  LLLKFKKWMSELIQGHKKGFQEDAEMNKRNEEKKFGMLGSHEDLSKSSLDRNQLAHNKQS
781  STRSSEDFHLNSFSNPPRQYQKIMKRLIKRYVLQAQIDKESDEVNEGELKEIKQDISSLR
841  YELLEEKSQNTEDLAELIRKLGERLSLESKQEESRR.
```

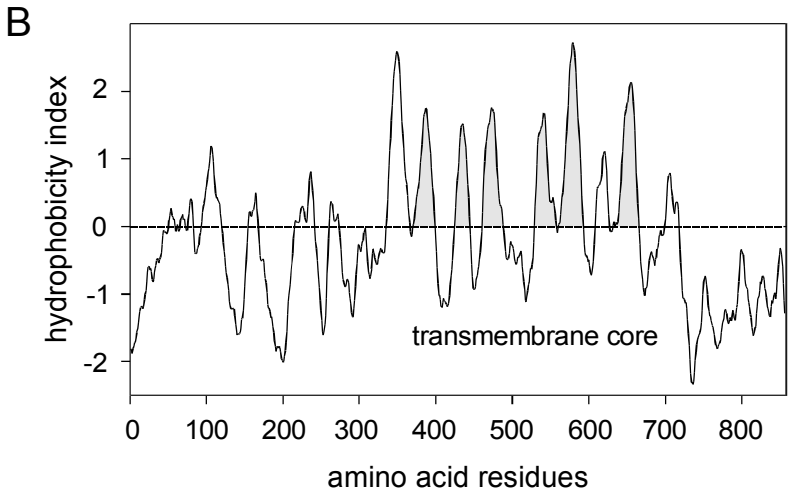

Fig. 25: **Primary structure and membrane topology of rat TRPC6.** *A*: Deduced amino-acid sequence of rat TRPC6 cloned from rat brain and A7r5 cells. *Underlined regions*: Putative ankyrin repeat domains*, grey boxes*: putative transmembrane (TM) segments (cf. *B*), b*oxes*: Amino acid exchanges with respect to the rSTRPC6B sequence published by Zhang & Saffen (2001), M757I, S767F. *B*: Hydrophobicity profile of rat TRPC6 as obtained by Kyte-Doolittle hydropathy analysis. The transmembrane core comprising TM1 – 6 is indicated *in grey*.

The rTRPC6 clone obtained in the present study is composed of 876 amino-acid residues (Fig. 25*A*). Unlike the sequences of mouse, canine and human TRPC6 (Boulay *et al*., 1997; Hofmann *et al*., 1999; Walker *et al*., 2001) that closely resemble rTRPC6A (Zhang & Saffen, 2001), the sequence of the rTRPC6 clone identified in the present study corresponds to rTRPC6B (Zhang & Saffen, 2001), with the exception of two

amino-acid exchanges in the C-terminal region: M757I and S767F. Compared with rTRPC6A, rTRPC6B lacks 54 amino acids near the start of the N terminus (Zhang & Saffen, 2001). Three putative ankyrin repeats are present in the N-terminal cytosolic region and the TRP domain is found in the proximal C terminus. The hydropathy profile (Fig. 25B) predicts seven hydrophobic regions (H1 – H7) which could potentially form transmembrane segments (TMs). By analogy with the findings on human TRPC3 (Vannier *et al*., 1998), H2 – H7 of rTRPC6 are believed to represent the six transmembrane segments, typical of TRP channels, with the putative pore-forming loop between TM5 and TM6.

3.2.2. Biophysical properties of rTPRC6 and mTRPC5

Receptor-activated currents through mTRPC5 and rTRPC6

Whole-cell voltage-clamp recordings were performed to compare currents mediated by rTRPC6 to those mediated by mTRPC5.

No constitutive activity was observed at a holding potential of -60 mV in the stable T-REx-r6 cell line after induction of rTRPC6 expression with tetracycline. Currents on break-in were in the range of -0.1 to -1.87 pA/pF ($n = 24$) and were not significantly different from those in control cells. When histamine (100 µM) was applied to tetracycline-treated T-REx-r6 cells transiently expressing the histamine H_1 receptor, large inward currents developed (Fig. 26*A*, $n = 9$). Despite the continued presence of the agonist, current decayed after reaching a maximum. Current decay was usually fast and removal of the agonist had no effect on the rate of current decay. As shown above for AVP-induced currents in A7r5 cells, rTRPC6-mediated inward currents could also be elicited by infusion of AlF_4^- (Fig. 26*B*, $n = 31$. In contrast to findings reported by Zhang & Saffen (2001), addition of the membrane-permeable diacylglycerol OAG (Fig. 26*C*, 100 µM, $n = 11$) to the bath solution also activated the current. According to Zhang & Saffen, only the longer isoform TRPC6A was stimulated by OAG. OAG- and AlF_4^--induced currents in T-REx-r6 cells were indistinguishable from agonist-induced currents with respect to the *I-V* relation, and their sensitivity to lanthanides and external Ca^{2+} (see below). Like the histamine-induced currents, currents elicited by OAG were relatively short-lived. By contrast, response kinetics were considerably slowed when AlF_4^- was used for current activation. As shown above for cation currents endogenous

to A7r5 cells and as reported previously for mouse (Inoue *et al*., 2001) and human (Hofmann *et al*., 1999) isoforms of TRPC6, the *I-V* relation of currents mediated by rTRPC6 (Fig. 26*D*) displayed a characteristic doubly-rectifying shape and reversal potentials close to 0 mV (Hofmann *et al*., 1999; Inoue *et al*., 2001), indicative of nonselective cation currents.

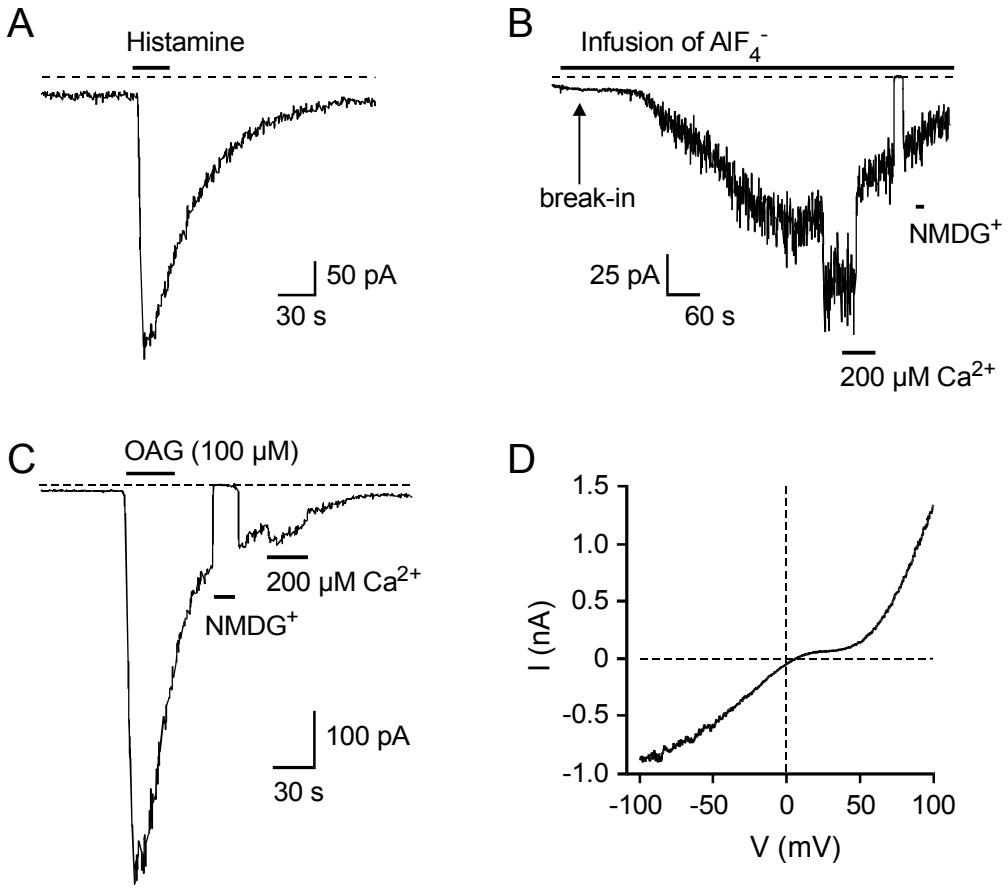

Fig. 26: **Whole-cell currents carried by rat TRPC6.** Whole-cell currents in T-REx cells stably transfected with rTRPC6 were recorded at a holding potential of -60 mV (*A*-*C*). Histamine (100 µM, *A*) or OAG (100 µM, *C*) were added to the extracellular solution as indicated by the bars. *B*: Currents elicited by infusion of AlF_4^-. *D*: *I-V* relationship of the OAG-induced current obtained during voltage ramps from -100 to +100 mV at the peak of the inward current shown in *C*.

Following patch rupture, many HEK293 cells co-expressing mTRPC5 and the histamine H_1 receptor showed an increased holding current at -60 mV (-3.5 ± 0.5 pA/pF, $n = 79$, C_m = -15.1 ± 0.7 pF) compared to that of control cells only expressing the histamine H_1 receptor (-1.0 ± 0.3 pA/pF, $n = 6$, C_m = -13.0 ± 1.0 pF). The noisy inward current observed upon break-in in most mTRPC5-expressing cells had a doubly-rectifying

shape characteristic of activated mTRPC5 (see below and compare Schaefer *et al*., 2000). These data suggest that mTRPC5 shows basal activity as described previously (Schaefer *et al*., 2000). When histamine (100 µM) was applied to HEK293 cells transiently co-expressing mTRPC5 and the H_1 receptor, transient inward currents (61.8 ± 8.6 pA/pF, $n = 31$, $C_m = -15.1 \pm 0.7$ pF) were evoked (Fig. 27*A*). Response decay was usually slower than that of currents mediated by rTRPC6. Upon removal of histamine, the currents rapidly returned to prestimulation levels.

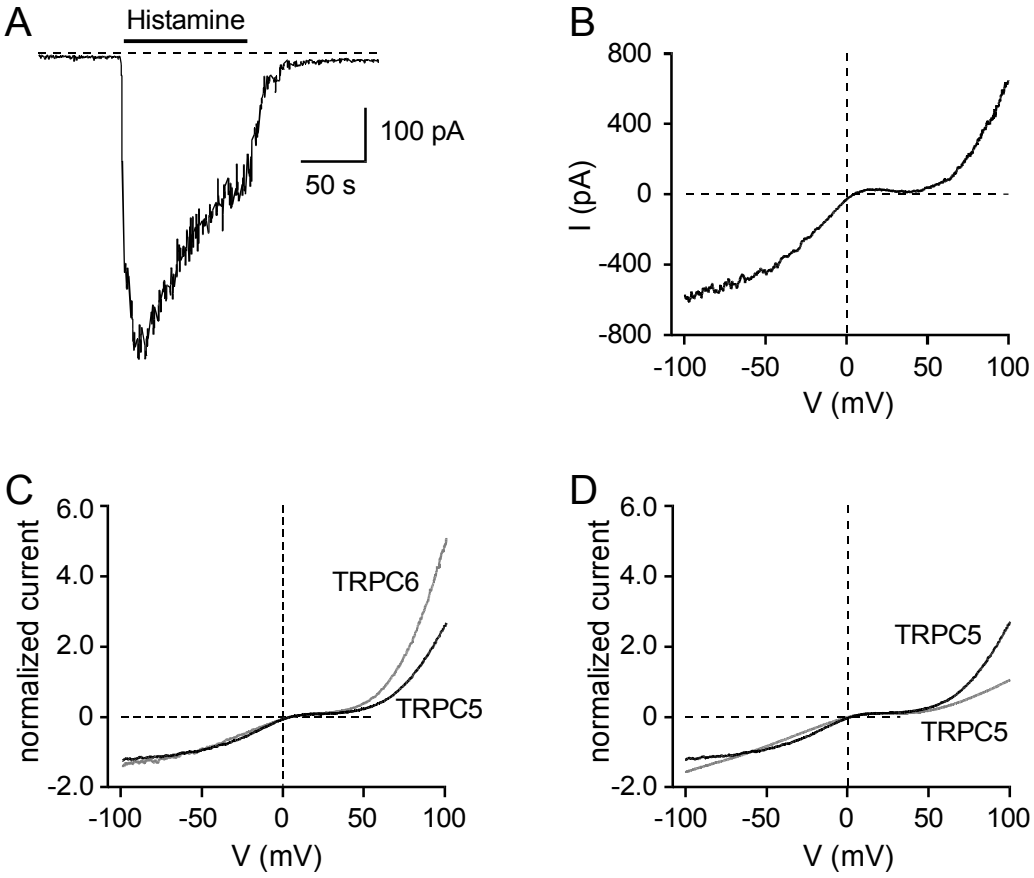

Fig. 27: *A*,*B*: **Whole-cell currents carried by mouse TRPC5**. *A*: Histamine (100 µM)-induced whole-cell current in mTRPC5-expressing HEK293 cells at a holding potential of -60 mV. *B*: Corresponding *I-V* relationship of the HA-induced current obtained during voltage ramps from -100 to +100 mV at the peak of the inward current shown in *A*. *C*, *D*: **Comparison of the *I-V* relations of mTRPC5 and rTRPC6 currents**. *C*: Normalized *I-V* relationships of mTRPC5 (*black trace*)- and rTRPC6 (*grey trace*)-mediated currents. Each curve is the mean of ten individual experiments. *D*: Comparison of normalized *I-V* relations typical for very large (> 2 nA at -60 mV, *grey trace*) and smaller (*black trace*) mTRPC5 currents. The *grey trace* is the mean of 6 individual experiments. The *I-V* relations were normalized to the current values obtained at -60 mV (*C*, *D*).

As reported previously (Schaefer *et al*., 2000), the *I-V* relation of the histamine-induced current in mTRPC5-expressing cells (Fig. 27*B*) was doubly rectifying and reversal potentials were close to 0 mV, indicative of nonselective cation currents. In control cells only expressing the histamine H_1 receptor, histamine application did not result in an increase in current in any of the cells tested, suggesting that the currents observed in TRPC5- and H_1 receptor-coexpressing cells are mediated by TRPC5. Control cells, however, did respond to histamine with increases in intracellular Ca^{2+}.

In Fig. 27*C*, the *I-V* relations of ten experiments for mTRPC5- and rTRPC6-expressing cells were normalized to the respective current values at -60 mV and the calculated mean curves superimposed. To obtain the mean *I-V* relationship for mTRPC5, only cells exhibiting currents < 2 nA at a holding potential of -60 mV were selected (see below). As illustrated in Fig. 27*C*, the *I-V* relations of currents mediated by mTRPC5 and rTRPC6 are very similar, although larger outward currents are observed in rTRPC6-expressing cells. Interestingly, when TRPC5 currents exceeded 1 – 2 nA at -60 mV, the shape of the *I-V* relation changed. In Fig. 27*D*, the normalized *I-V* relation typical of large currents is shown. Although the overall shape of the *I-V* relationship is similar, the proportion of inward current is increased and the *I-V* relation is linear below 0 mV. The reasons for the observed changes remain unclear.

The single-channel properties of mTRPC5 and rTRPC6 were characterised using the outside-out patch configuration. Under the same conditions used for whole-cell recordings, single-channel events of around -2.5 pA at a potential of -60 mV (Fig. 28*A* & Table 2) were observed in mTRPC5-expressing cells after stimulation with histamine (100 μM). To determine the voltage dependence of the single-channel amplitude for mTRPC5, in some recordings the membrane potential was stepped from -100 to +80 mV (Fig. 28*C*). Under the conditions used, patches tended to be less stable at positive potentials. In Fig. 28*D*, data from several individual recordings were pooled. The pooled *I-V* relationship of the single-channel currents mediated by mTRPC5 resembled that of whole-cell currents, showing a doubly-rectifying shape, as well as a reversal potential close to 0 mV. The mean open dwell time of histamine-induced mTRPC5 currents was ~ 8 ms (cf. Table 2). The single-channel chord conductance at -60 mV was 41.3 ± 1.1 pS (n = 12).

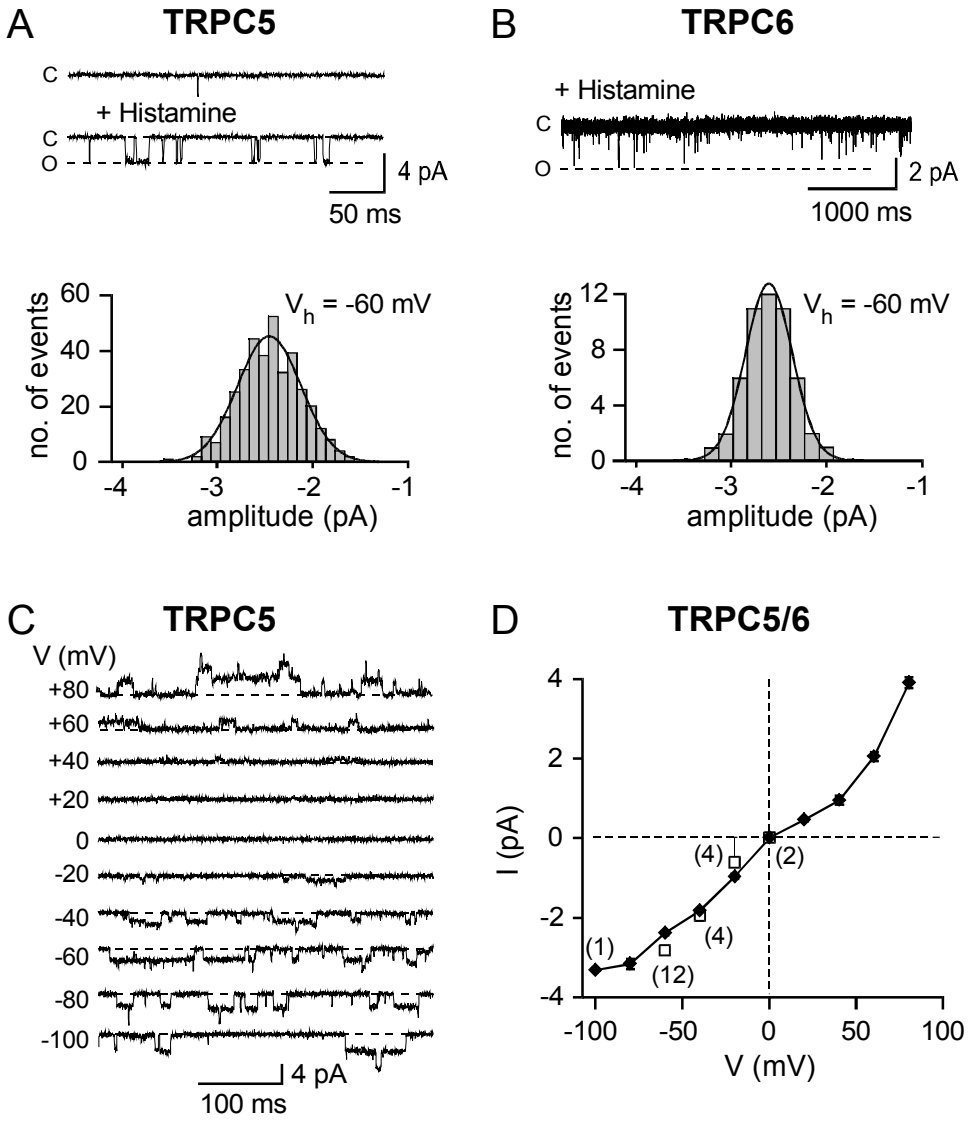

Fig. 28: **Single-channel properties of mouse TRPC5 and rat TRPC6 in outside-out membrane patches.** *A,B*: *upper panels*: current traces recorded in patches from H_1-, and TRPC5- or TRPC6-expressing cells at a membrane potential of -60 mV. Histamine (100 µM) was used to activate TRPC5 or TRPC6 channels. Open and closed levels are indicated by *o* and *c*, respectively. *Lower panels*: Corresponding amplitude histograms. *C:* Single-channel recordings for mTRPC5 obtained from a single patch at the indicated potentials. Closed levels are indicated by the *dotted line*. *D*: *I-V* relation of the mTRPC5 (*closed symbols*) and rTRPC6 (*open symbols*) single-channel current. The values are means ± S.E.M. (*error bars* as indicated). If not otherwise indicated the number of experiments is ≥ 4.

As reported previously for human TRPC6 (Hofmann *et al*., 1999), single-channel openings of rTRPC6, elicited by application of histamine or OAG, were typically of very short duration, with more than 70 % of the openings shorter than 0.5 ms. Hence, under the recording conditions used most openings of TRPC6 channels could not be

fully resolved. From openings longer than 2 ms, the amplitude of single-channel events at a holding potential of -60 mV was determined to be -2.81 ± 0.07 pA (*n* = 8, Fig. 28*B* & Table 1). Because, under the conditions used, patches were unstable at positive potentials, we limited the analysis of the potential dependence of single-channel currents mediated by rTRPC6 to potentials below 0 mV (Fig. 28*D*). The single-channel chord conductance at -60 mV was 46.6 ± 1.5 pS (*n* = 12) for rTRPC6.

Effects of $[Ca^{2+}]_o$ on currents mediated by TRPC5 and TRPC6

In view of the intriguing results obtained for the cation currents endogenous to A7r5 cells and the findings reported for different TRPC isoforms (Okada *et al*., 1998; Okada *et al*., 1999; Schaefer *et al*., 2000; Inoue *et al*., 2001), the effects of external Ca^{2+} on whole-cell currents mediated by mTRPC5 and rTRPC6 were studied. When $[Ca^{2+}]_o$ was decreased from physiological levels to 200 µM, histamine-induced currents in HEK293 cells co-expressing TRPC5 and the histamine H_1 receptor were rapidly and reversibly decreased (Fig. 29*A*). By contrast, a prominent potentiation of histamine-induced currents was observed in T-REx-r6 cells transiently co-transfected with the H_1 receptor (Fig. 29*B*). When $[Ca^{2+}]_o$ was increased from 2 mM to 20 mM currents mediated by mTRPC5 were reversibly increased (Fig. 29*C*) whereas currents through rTRPC6 channels were drastically decreased (Fig. 29*D*). In Fig. 30*A*,*B*, representative *I-V* relations of TRPC5 and TRPC6 currents in 200 µM and 2 mM Ca^{2+}-containing solutions are shown. The *I-V* relationships for both channels were similar in solutions containing high and low external Ca^{2+}. However, changes in $[Ca^{2+}]_o$ affected the amplitude of TRPC6 currents at all potentials to a similar extent, whereas for TRPC5, effects on inward currents were more pronounced. Moreover, the reversal potential of TRPC6 currents remained unchanged upon changes in $[Ca^{2+}]_o$, while for TRPC5 currents, the reversal potential was shifted toward more positive potentials when $[Ca^{2+}]_o$ was increased. The effects of different $[Ca^{2+}]_o$ on the amplitude of currents mediated by mTRPC5 and rTRPC6 is summarised in Figure 31. The data suggest that TRPC5 and TRPC6 are inversely regulated by $[Ca^{2+}]_o$, with currents mediated by TRPC5 increasing and currents mediated by TRPC6 decreasing with increasing $[Ca^{2+}]_o$. In contrast to the findings on regulation of cation currents in A7r5 cells by external Ca^{2+}, the effects of

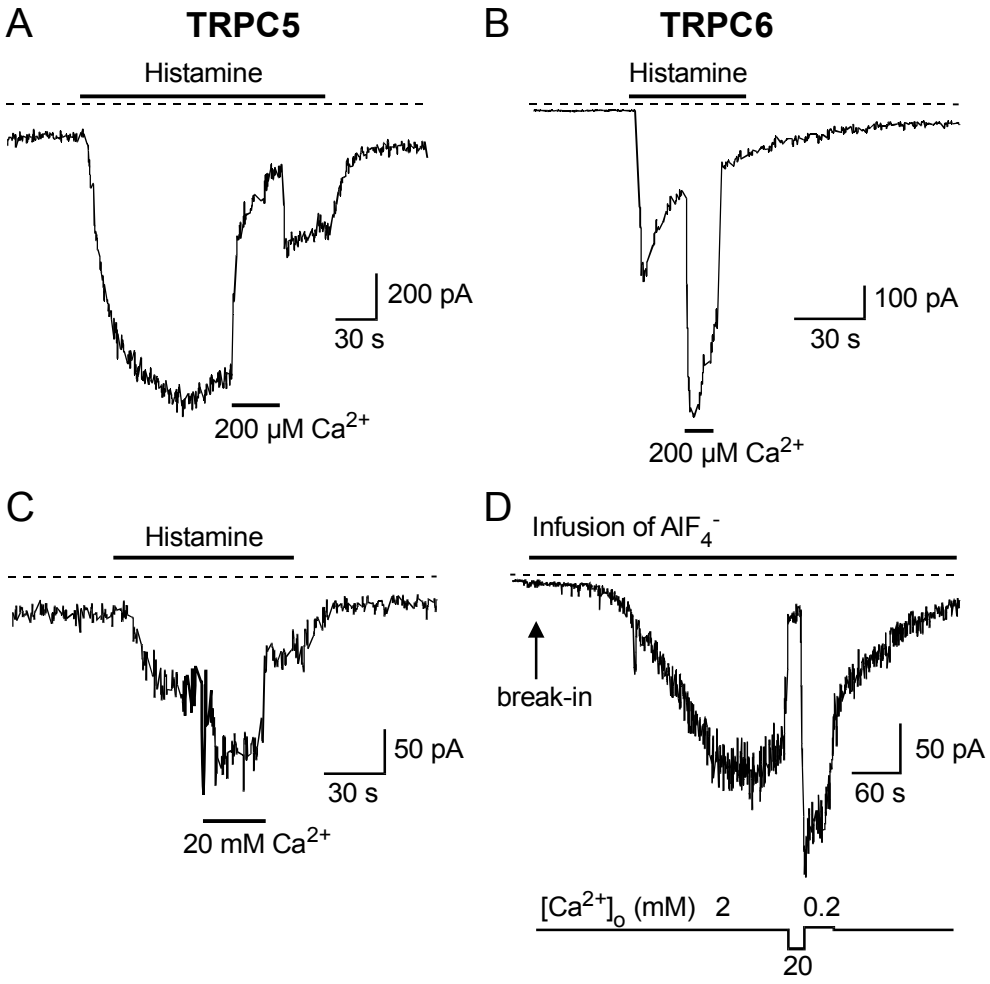

Fig. 29: **Opposite effects of Ca_o^{2+} on currents mediated by mouse TRPC5 and rat TRPC6.** *A*,*C*: Effects of decreasing (*A*) or increasing (*C*) $[Ca^{2+}]_o$ on inward currents at -60 mV elicited by histamine (100 µM) in mTRPC5-expressing HEK293 cells. *B*,*D*: Effects of decreasing (*B*) or increasing (*D*) $[Ca^{2+}]_o$ on inward currents at -60 mV in rTRPC6-expressing T-TREx-293 cells. Inward currents were elicited by histamine (100 µM, *B*) or by infusion of aluminium fluoride (AlF_4^-, *D*).

Ca^{2+} on rTRPC6 currents seemed to be solely inhibitory. No potentiating actions of external Ca^{2+} were revealed when relative current amplitudes in nominally Ca^{2+}-free and 200 µM Ca^{2+}-containing solutions were compared (Fig. 31). Accordingly, when histamine-induced currents in rTRPC6-expressing cells were elicited in $[Ca^{2+}]_o$ = 200 µM, acute Ca_o^{2+} removal did not change the amplitude of the current response (n = 3, *data not shown*).

Single-channel recordings were performed to study the effects of changes in $[Ca^{2+}]_o$ on rTRPC6 channels in more detail. As can be concluded from Fig. 32*A*,*C*, decreasing the

$[Ca^{2+}]_o$ from physiological levels to 200 µM prominently increased the frequency of channel openings. Increasing $[Ca^{2+}]_o$ to 20 mM had opposite effects. In this case, the frequency of channel openings was reversibly decreased (Fig. 32*B*,*D*). Statistical analysis of the data is presented in Table 1. With respect to the channel conductance, no changes could be observed when $[Ca^{2+}]_o$ was decreased to 200 µM (Table 1). However, changing the $[Ca^{2+}]_o$ to 20 mM significantly ($P < 0.05$) reduced the single-channel chord conductance at -60 mV from about 47 pS to about 36 pS (Table 1).

Hence, the above data suggests that $[Ca^{2+}]_o$ modulates the frequency of channel openings as well as the single-channel conductance of rTRPC6-mediated currents.

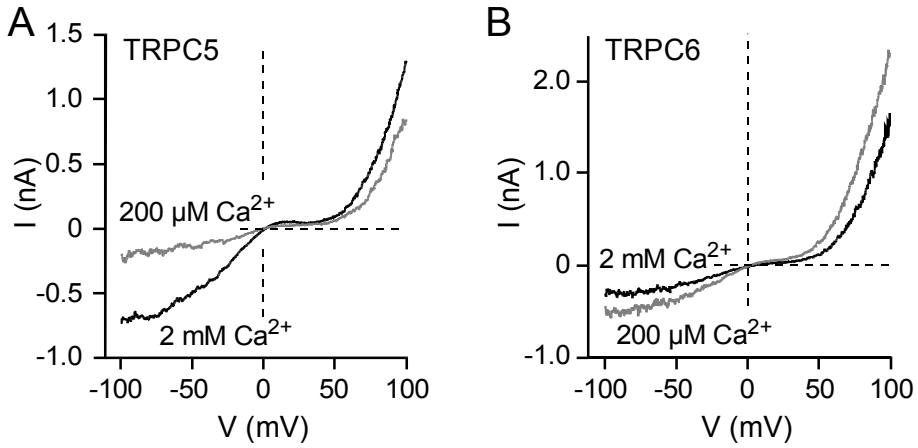

Fig. 30: **Comparison of the *I-V* relations of the currents mediated by mouse TRPC5 and rat TRPC6 in physiological and in reduced $[Ca^{2+}]_o$.** *I-V* relations in 2 mM (*black traces*) and in 200 µM (*grey traces*) Ca^{2+}-containing solutions recorded from mTRPC5-expressing HEK293 cells (*A*) or rTRPC6-expressing T-TREx-293 cells (*B*) upon stimulation by histamine or OAG, respectively. The *I-V* relations were obtained during voltage ramps from -100 to +100 mV.

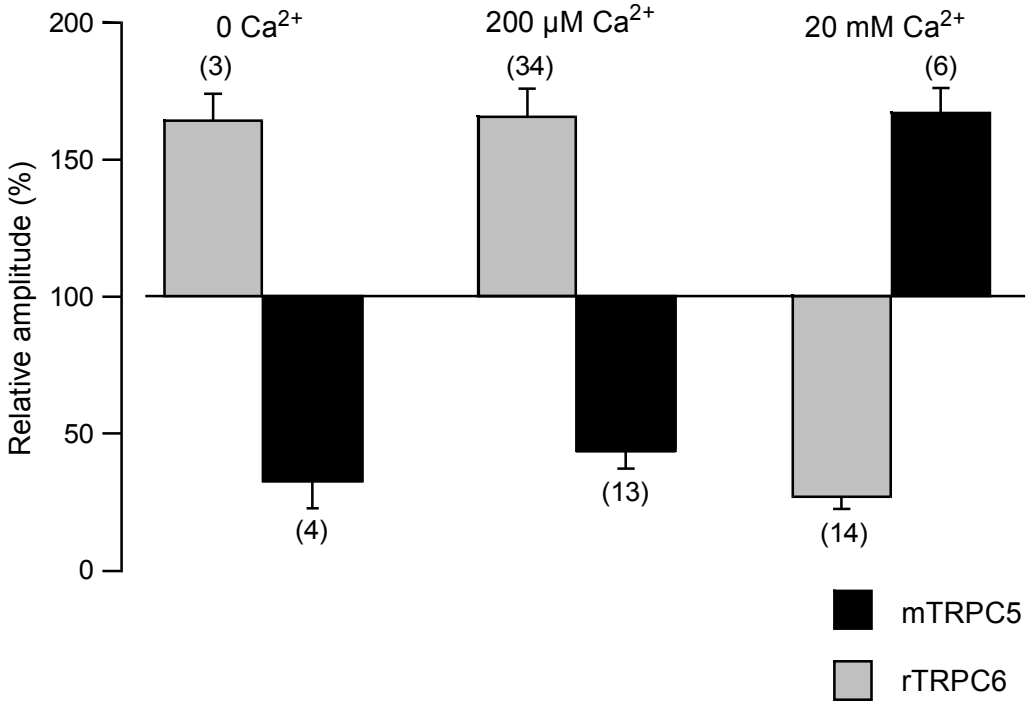

Fig. 31: **Statistical analysis of $[Ca^{2+}]_o$ effects on whole-cell currents mediated by mouse TRPC5 and rat TRPC6.** Relative amplitudes of whole-cell currents at -60 mV were calculated with respect to the amplitude values in 2 mM Ca_o^{2+} (100 %). The number of experiments are indicated in parentheses. *Errors bars* represent S.E.M..

Table 1: Effects of different external Ca^{2+} concentrations on the single-channel properties of recombinant rat TRPC6

$[Ca^{2+}]_o$ (V_h = -60 mV)	*i* (pA)	(n)	frequency (Hz)	(n)
2 mM Ca^{2+} (physiological)	-2.81 ± 0.07	(8)	22.3 ± 4.9	(8)
200 µM Ca^{2+}	-2.91 ± 0.12	(6)	43.4 ± 13.9*	(6)
20 mM Ca^{2+}	-2.16 ± 0.11*	(3)	2.4 ± 1.0**	(3)

* $P < 0.05$, ** $P < 0.01$ compared with the values at physiological $[Ca^{2+}]_o$ (To test for significant differences between the mean values, paired t test was used, i.e. only values obtained in the same recording were compared.)

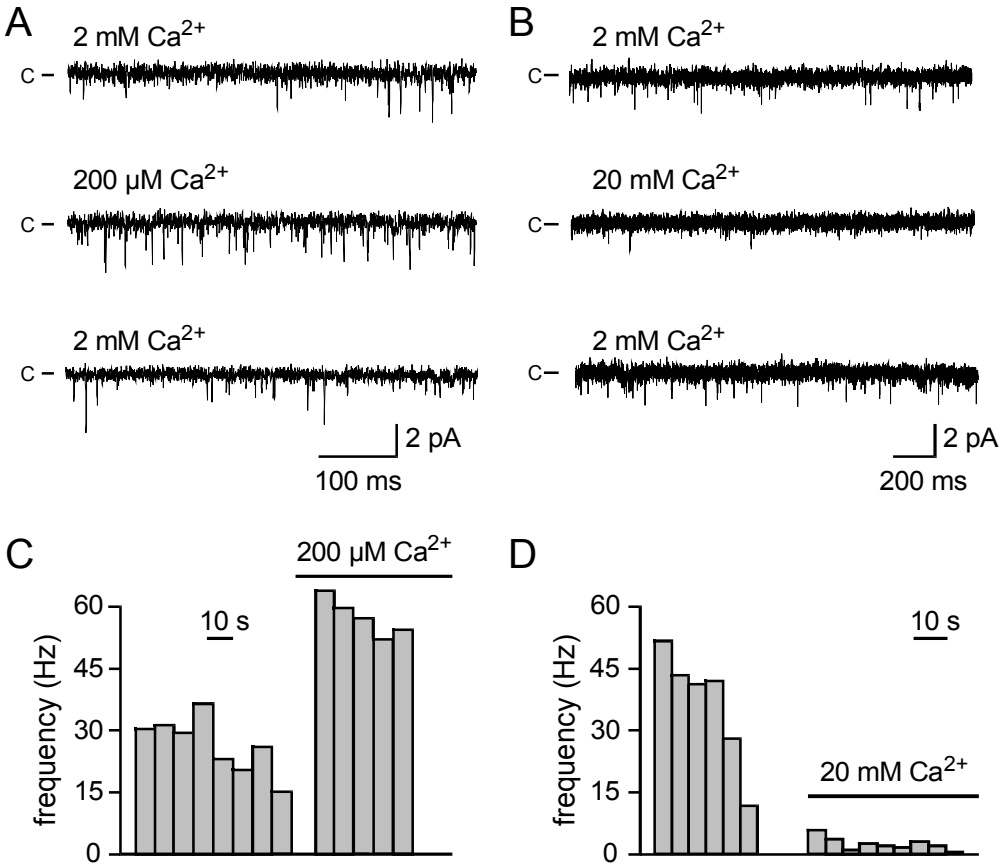

Fig. 32: **Effects of decreased and increased $[Ca^{2+}]_o$ on single-channel currents mediated by rat TRPC6.** Effects of decreasing $[Ca^{2+}]_o$ from physiological levels to 200 µM (*A*) or increasing $[Ca^{2+}]_o$ from physiological levels to 20 mM (*B*) on rTRPC6 single-channel activity in outside-out patches from T-Rex-r6 cells at a holding potential of –60 mV. *C*, *D*: channel activity expressed as opening frequency over time (calculated for consecutive 5-s periods).

Effects of lanthanides on currents mediated by TRPC5 or TRPC6

The effects of lanthanides on currents mediated by mTRPC5 and rTRPC6 were compared. When, during exposure to histamine (100 µM), La^{3+} (10 µM) was applied to HEK293 cells co-expressing mTRPC5 and the histamine H_1-receptor, inward and outward currents were strongly increased (Fig. 33*A*). Likewise, in Ca^{2+} imaging experiments, micromolar concentrations of La^{3+} applied during histamine-induced $[Ca^{2+}]_i$ increases resulted in enhanced response amplitudes, suggesting an increased Ca^{2+} influx under these conditions ($n = 7$, Fig. 33*C*, *inset*). Comparison of the *I-V* relation before and after application of La^{3+} revealed that the potentiating effect of La^{3+} was much more pronounced at negative potentials (Fig. 33*C*). Because La^{3+} is already effective at very low concentrations, a role for La^{3+} as a charge carrier for the additional

inward currents can be excluded. This conclusion is confirmed by the fact that no shift in the reversal potential of the current was detected. In control cells only transfected with the histamine H_1 receptor, neither application of histamine nor subsequent addition of La^{3+} resulted in a current increase ($n = 6$). In these cells, application of La^{3+} decreased basal leak currents rather than causing potentiation. The above data suggest that La^{3+} indeed affects currents carried by TRPC5. By contrast, when La^{3+} (100 µM) was applied to rTRPC6-expressing T-REx-r6 cells stimulated with OAG (100 µM), rapid inhibition of the inward current was observed at a holding potential of -60 mV (Fig. 33*B*). Inhibition was almost complete at all potentials tested (Fig. 33*B*, *inset* and Fig. 33D). For both TRPC5- and TRPC6-mediated currents, the effects of lanthanides were readily reversible on wash-out.

To analyse the effects of lanthanides on TRPC5- and TRPC6-mediated currents in more detail, cells were exposed to various concentrations of La^{3+} or Gd^{3+} (Fig. 34*A*,*B*). Because agonist- and OAG-induced currents in T-REx-r6 cells were relatively short-lived, infusion of aluminium fluoride (AlF_4^-) via the pipette was preferred. With AlF_4^-, response kinetics were considerably slowed, thus allowing the effects of different concentrations of the lanthanides to be investigated in the same cell. The data obtained for different concentrations of the respective lanthanides were pooled to establish the concentration-response relationships for TRPC5- and TRPC6-mediated currents (Fig. 34*C,D*). The inhibitory effect of lanthanides on rTRPC6 began at concentrations around 1 µM, and 1 mM [La^{3+}] resulted in near complete inhibition. The concentration-response relationship for La^{3+} inhibition of rTRPC6 was sigmoidal (Fig. 34*C*) and fitted by the Hill equation with an IC_{50} value of 6.1 µM. The effects of Gd^{3+} on currents mediated by TRPC6 were examined at only two different concentrations, 10 µM and 1 mM. The values for relative inhibition by Gd^{3+} were similar to those obtained with La^{3+}. As shown in Figure 34*D*, the effects of La^{3+} and Gd^{3+} on currents mediated by TRPC5 were more complex. Starting at a concentration of around 1 µM, both La^{3+} and Gd^{3+} increased TRPC5-mediated currents in a concentration-dependent manner. The largest potentiation was observed between 10 µM and 1 mM. At concentrations > 1 mM, the potentiating effect was reduced or in the case of La^{3+} even reversed (Fig. 34*B*, *Inset*). The mean relative current amplitude in 5 mM Gd^{3+} was approximately 120 %, suggesting minor augmentative effects on TRPC5-mediated currents.

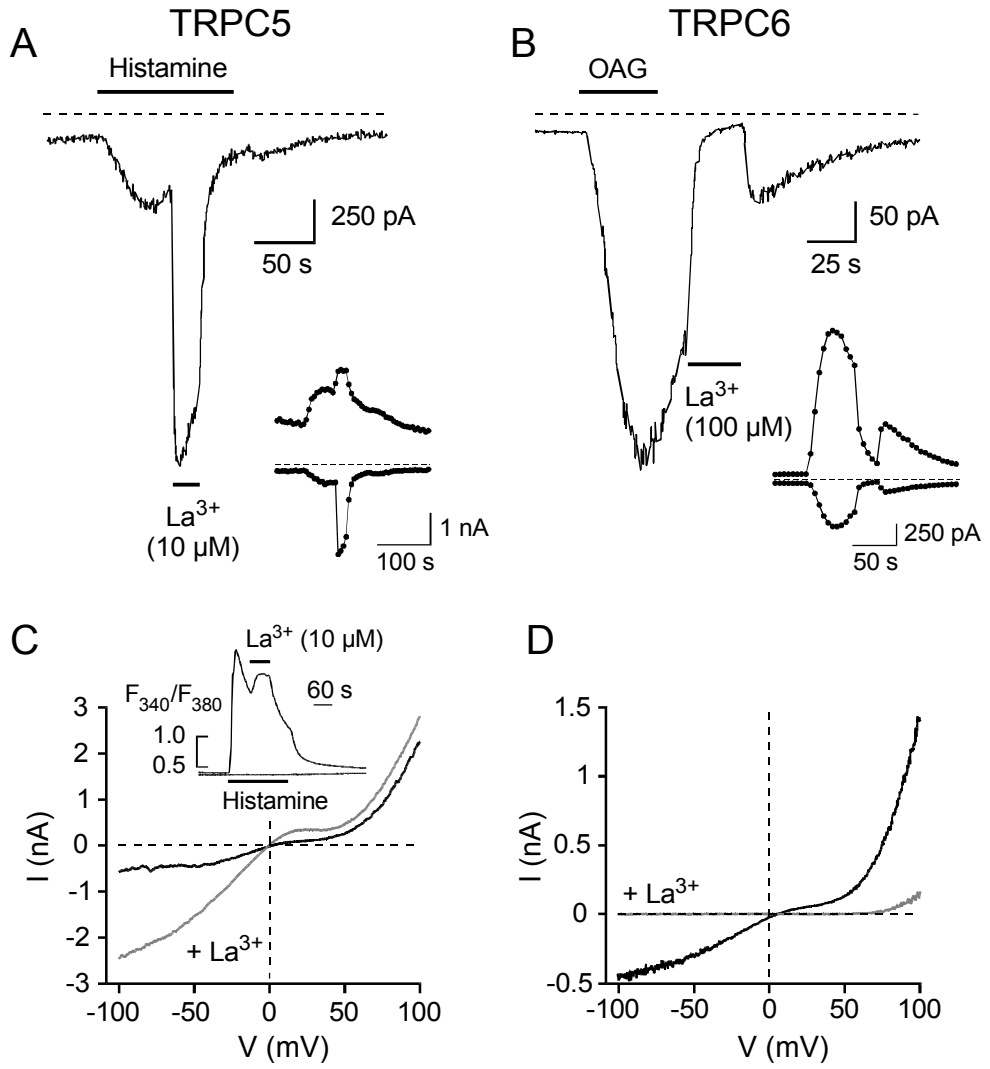

Fig. 33: **Opposite effects of bath application of La^{3+} on currents mediated by mouse TRPC5 and rat TRPC6**. *A*: Potentiating effects of La^{3+} (10 µM) on inward currents elicited by histamine (100 µM) in mTRPC5-expressing HEK293 cells at a holding potential of -60 mV. *Inset:* Whole-cell currents at -100 and +100 mV. *C*: Corresponding *I-V* relationships in the presence (*grey trace*) and absence (*black trace*) of La^{3+}. *Inset*: Effects of La^{3+} (10 µM) on histamine-induced Ca^{2+} responses of fura-2-loaded HEK293 cells co-expressing mTRPC5 and the rat H_1 receptor (GFP-positive). Unresponsive control cells (GFP-negative) recorded simultaneously from the same coverslip are shown as a control. The traces are the mean of 4 cells. *B*: Inhibitory effects of La^{3+} (100 µM) on inward currents elicited by OAG (100 µM) in rTRPC6-expressing T-REx-293 cells at a holding potential of -60 mV. *Inset:* Whole-cell currents at -100 and +100 mV. *D*: Corresponding *I-V* relationships in the presence (*grey trace*) and absence (*black trace*) of La^{3+}.

It has to be noted, however, that the effects of 5 mM Gd^{3+} on TRPC5-mediated currents were not uniform. Some cells responded with potentiation of currents (n = 2/5) whereas others responded with current inhibition (n = 3/5). Thus, lanthanides inhibit rTRPC6,

but have dual effects on mTRPC5. Low concentrations stimulate mTRPC5 currents, whereas high concentrations are less effective and may result in inhibition.

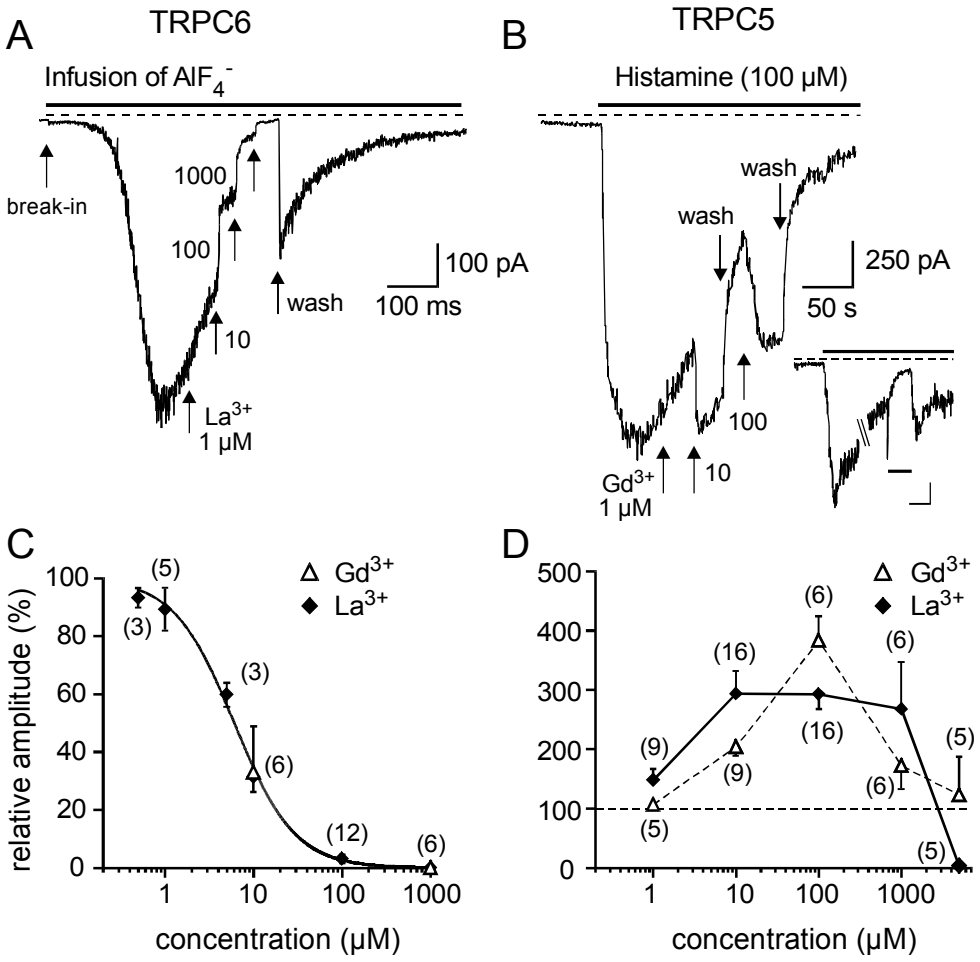

Fig. 34: **Concentration-response relationship of lanthanide effects on mouse TRPC5 and rat TRPC6.** *A:* Concentration-dependent block by La^{3+} of whole-cell currents elicited by infusion of AlF_4^- in rTRPC6-expressing T-REx-293 cells at -60 mV. *B:* Concentration-dependent increase by Gd^{3+} of whole-cell currents elicited by application of histamine (100 µM) in mTRPC5-expressing HEK293 cells at -60 mV. *Inset*: Inhibition of HA-induced currents by 5 mM La^{3+}. *Scale bars*: 30 s, 50 pA. *C*: Concentration-response curve for La^{3+} inhibition (*filled symbols*) of rTRPC6 currents. Mean inhibition values for Gd^{3+} are given by *open symbols* (n = 3). Relative amplitudes in La^{3+}-containing solutions were calculated with respect to current amplitudes in the absence of the blocker. IC_{50} value (~ 6 µM) for La^{3+} inhibition was obtained by fitting the data with the Hill equation. *D*: Concentration-response curve for La^{3+} (*filled symbols*) and Gd^{3+} (*open symbols*) effects on currents carried by mTRPC5. Relative changes were calculated as in *C*.

In general, the actions of lanthanides on ion channel behaviour are considered to be strictly confined to the extracellular face of the plasma membrane. However, a recent report on lanthanide-induced inhibition of currents mediated by human (h)TRPC3

transiently expressed in CHO cells, suggested intracellular regulatory actions for both La^{3+} and Gd^{3+}, though additional extracellular effects could not be excluded (Halaszovich *et al*., 2000). Lanthanides penetrated the cells by an unknown pathway not associated with the expressed channel. If the effects of lanthanides on TRPC6- and TRPC5-mediated currents resulted from an intracellular action of the free cation they should depend on the trivalent cation buffering capacity of the intracellular solution. Thus, raising the buffer capacity of intracellular solution by replacement of 10 mM EGTA, which itself binds La^{3+} and Gd^{3+} more strongly than Ca^{2+}, by 30 mM BAPTA should reduce the lanthanide effects on TRPC5 and TRPC6. The free Ca^{2+} concentration of both pipette solutions was kept at 100 nM. As seen in Fig. 35*A*,*C*, however, La^{3+} (10 μM) was still able to increase histamine-induced TRPC5 currents strongly under these experimental conditions. The relative increase of TRPC5-mediated currents was even more pronounced (7-fold, $n = 4$) when BAPTA replaced EGTA (cf. Fig. 34*D*) in the pipette solution. Interestingly, the amplitude of histamine-induced TRPC5 currents were reduced in BAPTA-containing pipette solutions (-4.5 ± 3.2 pA/pF, $n = 4$, $C_m = 21.9 \pm 5$, $P < 0.05$) confirming earlier reports indicating that TRPC5-mediated currents are dependent on $[Ca^{2+}]_i$ (Okada et al., 1998). In the presence of intracellular BAPTA, the inhibitory effect of La^{3+} (inhibition by 89.5 ± 2.2 %, $n = 4$, Fig. 35*B*,*D*) on inward currents through rTRPC6 was similar to that in EGTA (96.8 ± 1.5 %, $n = 12$). However, outward currents were blocked to a lesser extent.

To clarify the mechanism(s) underlying dual regulation of TRPC5-mediated currents by lanthanides, the effects of La^{3+} on the single-channel level were studied. When La^{3+} was added to the bath solution at a concentration of 100 μM, the open probability of mTRPC5 was dramatically increased (Fig. 36*A*). At the same time, the single-channel amplitude was approximately halved compared to that recorded before the addition of La^{3+} (Fig. 36*A*). Reduction of single-channel amplitudes of mTRPC5-mediated currents by application of 100 μM La^{3+} was observed at all potentials (Fig. 37*A,B*). The characteristic doubly-rectifying shape of the *I-V* relationship of TRPC5-mediated currents and the reversal potential around 0 mV were preserved in the presence of La^{3+} (Fig. 37*B*).

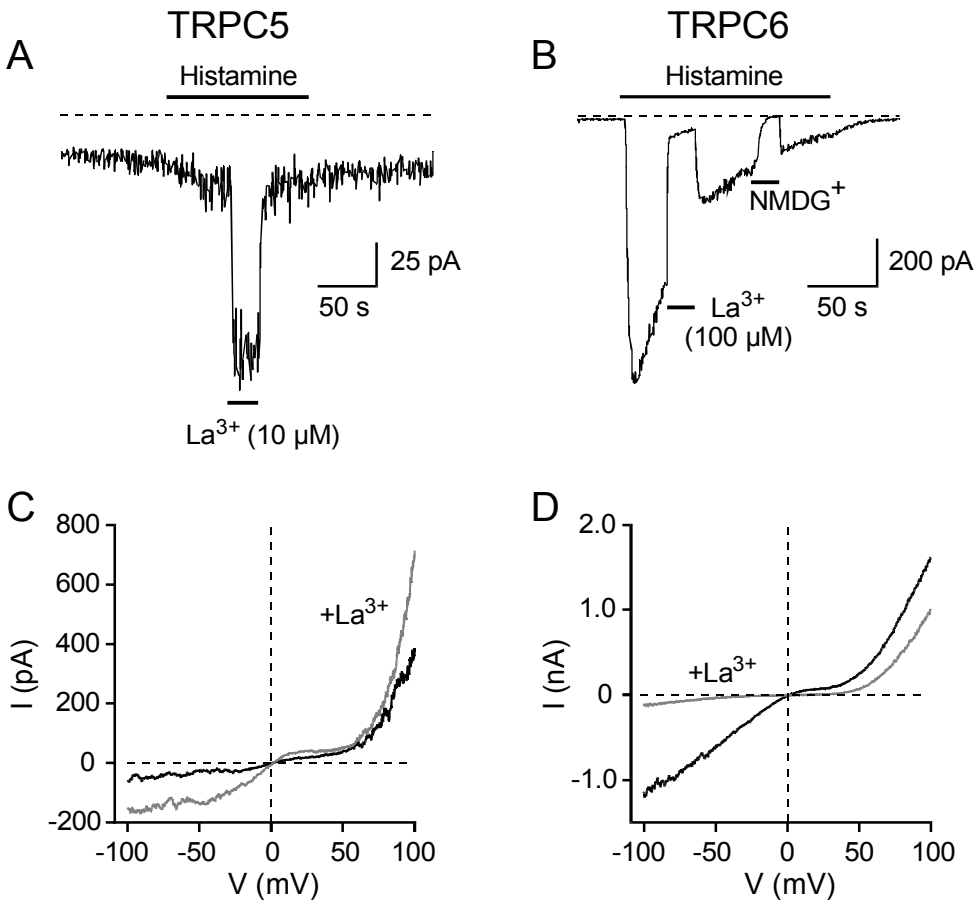

Fig. 35: **Effect of increased intracellular Ca^{2+} buffering on La^{3+} effects on currents mediated by mouse TRPC5 or rat TRPC6.** *A*, *B*: The pipette solution contained 30 mM BAPTA. *A*: Potentiating effects of 10 µM La^{3+} on inward currents elicited by histamine (100 µM) in mTRPC5-expressing HEK293 cells at -60 mV. *B*: Inhibitory effects of 100 µM La^{3+} on inward currents elicited by histamine (100 µM) in rTRPC6-expressing T-REx-293 cells at -60 mV. *I-V* relationships of mTRPC5 (*C*) or rTRPC6 (*D*) currents in the presence (*grey traces*) and absence (*black traces*) of La^{3+}.

The effects of different La^{3+} concentrations on single-channel amplitude is shown in Fig. 37*C*. Increasing the La^{3+} concentration from 1 µM to 5 mM resulted in a successive reduction of single-channel conductance. Single-channel properties including single-channel amplitude, open probability, mean open time and opening frequency were determined for different La^{3+} concentrations and the mean values calculated. The data are summarized in Table 2. It is evident from Table 2 that increasing La^{3+} concentrations led to a progressive reduction of single-channel conductance. By contrast, the open probability was roughly doubled in the presence of 1 µM La^{3+} and

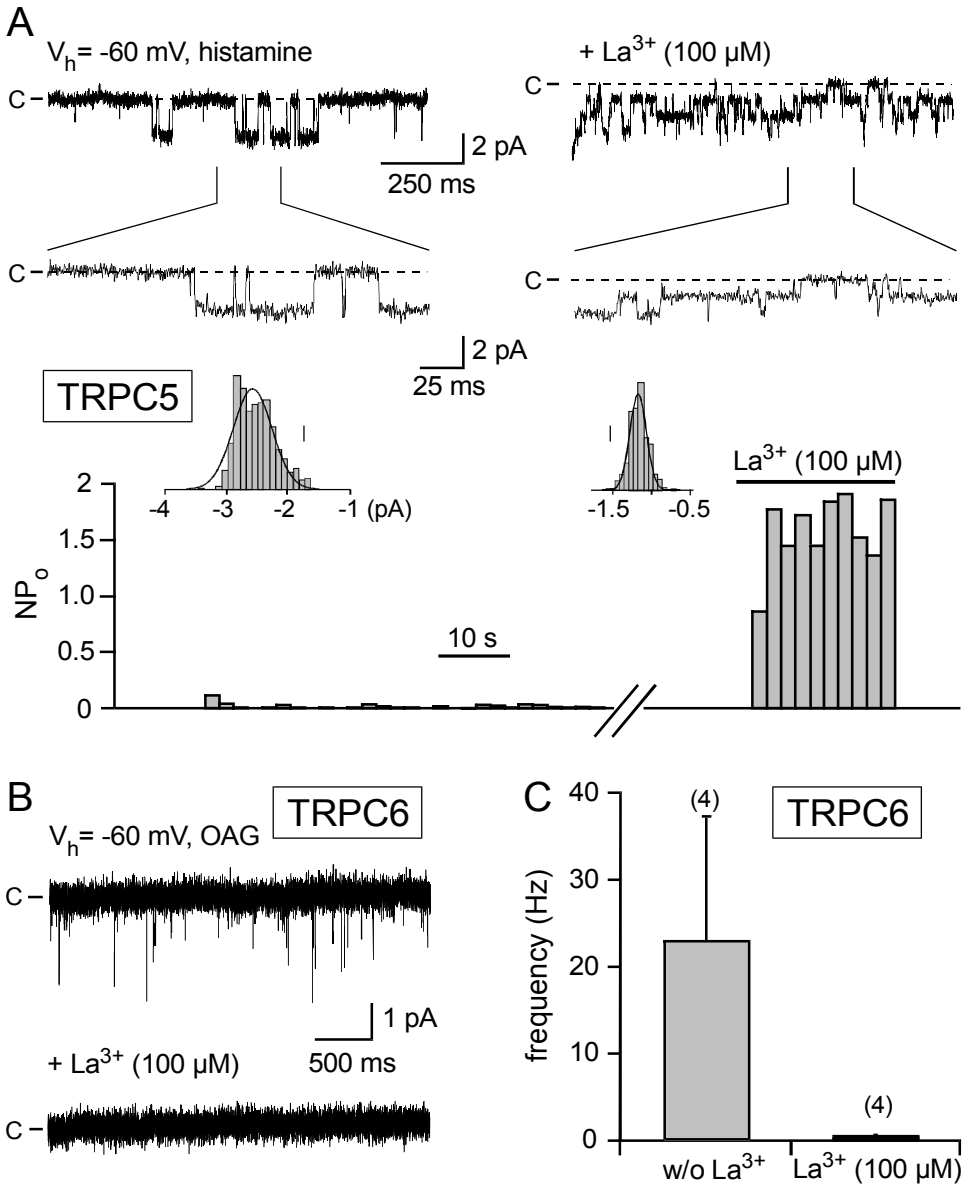

Fig. 36: **Effects of La^{3+} (100 µM) on single-channel currents mediated by mouse TRPC5 and rat TRPC6.** *A:* Outside-out patch recordings of mTRPC5-expressing HEK293 cells at a holding potential of -60 mV. *Upper panels*: Records of histamine-induced mTRPC5 single-channel currents before (*left traces*) and during addition of La^{3+} (100 µM) at two different resolutions. *Lower panels*: Channel activity expressed as open probability (NP_o) over time. *Inset:* Amplitude histograms obtained from the respective current traces. The vertical line indicates 10 or 4 events, respectively. *B:* Current traces recorded in outside-out patches from rTRPC6-expressing cells at a membrane potential of -60 mV before (*upper trace*) or during (*lower trace*) application of La^{3+}. C: Statistical analysis of La^{3+} (100 µM) effects on the opening frequency of rTRPC6 channels.

increased about tenfold in the presence of 100 µM La^{3+}. The last two columns of Table 2 show that the increased open probability of mTRPC5 channels in the presence of La^{3+} was due to increased open times and higher frequency of channel openings. It is

noteworthy that the fraction of channel openings excluded from the analysis (< 0.5 ms, see Material & Methods) decreased with increasing concentrations of La^{3+}. The respective percentage values for 'too short' events were included in Table 2. Accordingly, the relative increases in the mean open time obtained for different La^{3+} concentrations are probably underestimated. The combined effects of the increase in NP_o and the decrease in single-channel current was an approximately 10-fold increase in the total current through the patch (i x NP_o). Interestingly, the increase in patch current had a near identical dependence on the La^{3+} concentration to the whole-cell current. From the single-channel data, the EC_{50} for stimulation by La^{3+} was around 3 µM, whereas a 50 % reduction in the single-channel current occurred at a La^{3+} concentration of 100 µM. Owing to the limits of the resolution, the open probability of TRPC5 channels in the presence of La^{3+} at millimolar concentrations could not be determined. Taken together, the above data suggests that La^{3+} exerts diverse effects on single-channel activity inversely affecting channel conductance and open probability.

Because of the short mean open times of currents mediated by rTRPC6 no detailed analysis of lanthanide effects on single-channel kinetics was performed. Accordingly, only the effect of one La^{3+} concentration was studied. As shown in Fig. 36*B*,*C*, application of La^{3+} at a concentration of 100 µM, almost completely abolished channel opening.

In conclusion, in the absence of channel-specific pharmacological tools, the characteristic doubly-rectifying *I-V* relation, the markedly different single-channel open dwell times, and more importantly, the opposite effects of Ca_o^{2+} and of micromolar concentrations of La^{3+} and Gd^{3+} may be used to identify and discriminate contributions of TRPC4/5 and TRPC3/6/7 to receptor-operated cation currents in native tissues.

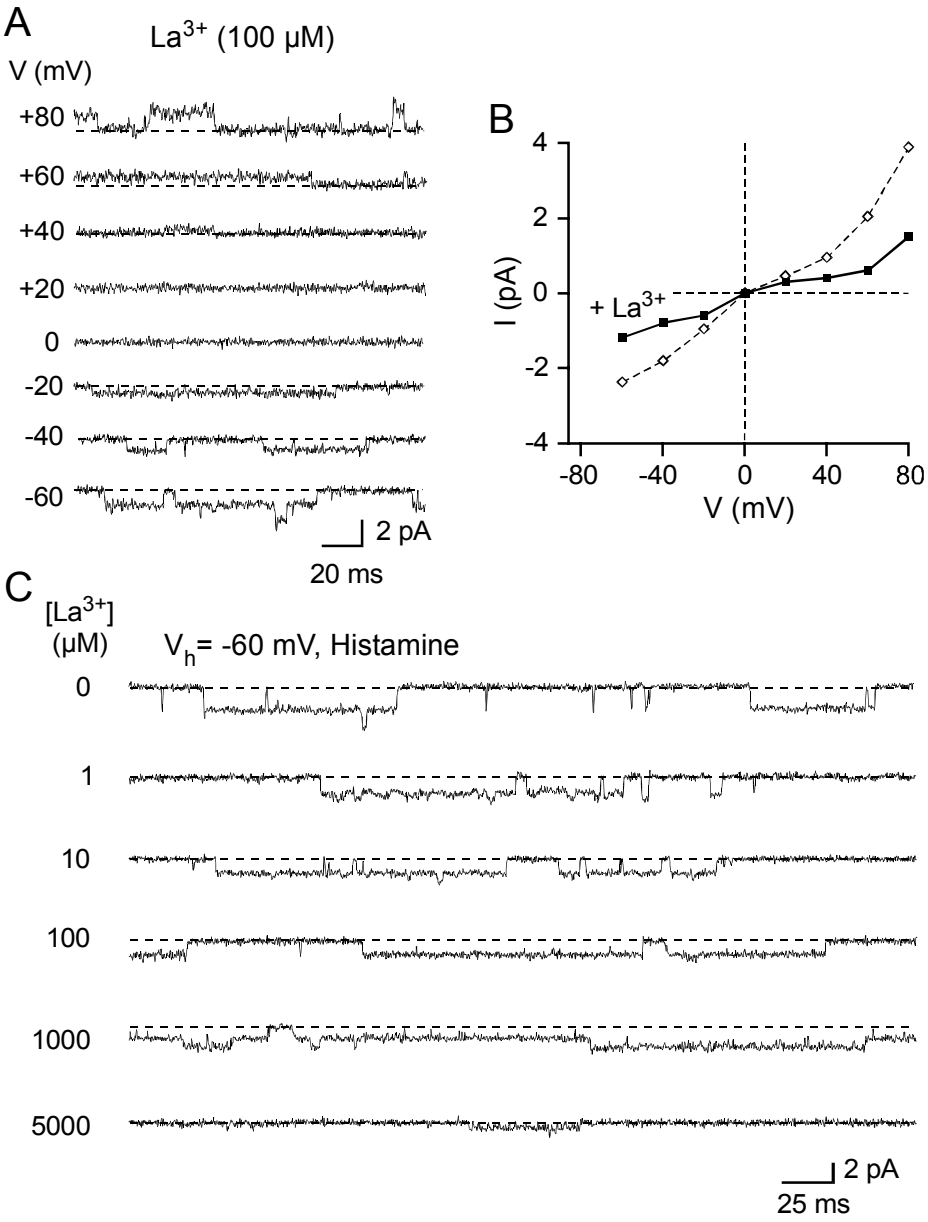

Fig. 37: **Potential dependence and concentration dependence of La^{3+} effects on single-channel currents mediated by mouse TRPC5.** *A*: Records of single-channel currents for mTRPC5 obtained at the indicated potentials in the presence of 100 µM La^{3+}. The traces were recorded from the same outside-out membrane patch. *B*: *I-V* relation of the single-channel current calculated from the recordings displayed in *A* (*black trace*). For comparison, the single-channel *I-V* relation from Fig. 28*D* is superimposed (*grey trace*). *C*: Sample traces from single-channel recordings obtained at the indicated concentrations of La^{3+} in different outside-out membrane patches from mTRPC5-expressing cells at a holding potential of -60 mV. *Dotted lines*: closed levels.

Table 2: Effect of different La^{3+} concentrations on the single-channel properties of heterologously expressed mTRPC5

	i (pA)	NP_o	mean open time (ms)	frequency (Hz)	(n)
-60 mV /HA	-2.48 ± 0.07 (n = 12)	0.06 ± 0.03	7.5 ± 2.8 (32.4 ± 3.7 %)	6.2 ± 1.7	(8)
$+La^{3+}$ (1 µM)	-1.85 ± 0.03 (n = 4)	0.15 ± 0.06	9.2 ± 2.2 (23.9 ± 4.6 %)	21.5 ± 8.0	(3)
$+La^{3+}$ (10 µM)	-1.44 ± 0.03 (n= 5)	0.94 ± 0.32	27.4 ± 7.5 (14.9 ± 2.9 %)	64.9 ± 32.0	(3)
$+La^{3+}$ (100 µM)	-1.31 ± 0.03 (n = 8)	1.13 ± 0.65	41.2 ± 19.4 (11.3 ± 1.6 %)	47.1 ± 18.4	(5)
$+La^{3+}$ (1 mM)	-1.17 (n = 1)	1.09 (n = 1)	23.4 (16.8 %)	n.d.	-/-
$+La^{3+}$ (5 mM)	-0.74 ± 0.02 (n = 3)	n.d.	n.d.	n.d.	-/-

HA: histamine. The values given in parentheses in the third column designate the percentage of events shorter than 0.5 ms (which have not been included into the statistics for open dwell time, open probability and amplitude, see Material & Methods). The values in the last column designate the number of experiments for the calculation of NP_o, mean open time and frequency at the respective concentration of La^{3+}.

3.2.3. Biophysical properties of chimaeric TRPC6-5

Chimaeric TRPC channels, in which corresponding parts of different TRPC channel isoforms are fused to give a new protein, may be valuable tools for structure-function analyses. However, to date, no studies on chimaeric TRPC channel isoforms exist. Because TRPC5 and TRPC6 were found to exhibit distinct biophysical properties, chimaeric TRPC6-5 channels provided by Dr. Michael Schaefer were electrophysiologically characterized. These channels consisted of the N-terminal portion of human TRPC6 (covering the transmembrane core up to the TRP box (EWKFAR)) and the corresponding C-terminal part of murine TRPC5 and could, thus, aid to clarify the role of the C-terminal regions of TRPC5 and TRPC6 for channel properties.

In HEK293 cells transiently co-expressing TRPC6-5 and the histamine H_1 receptor, histamine was found to elicit noisy inward currents (-114.2 ± 22.1 pA/pF, $n = 9$, C_m = -14.7 ± 1.9 pF) at a holding potential of -60 mV (Fig. 38*A*,*C*). Currents on break-in were –1.2 ± 0.2 pA/pF ($n = 9$, C_m = -14.7 ± 1.9 pF) and were not significantly different from those in control cells (-1.0 ± 0.3 pA/pF, $n = 6$, C_m = -13.0 ± 1.0 pF). Histamine-induced currents displayed a characteristic doubly-rectifying *I-V* relation (Fig. 38*B*,*D*) that resembles that of currents mediated by both TRPC5 and TRPC6. Like currents mediated by rat TRPC6, TRPC6-5 currents were reversibly increased upon reduction of $[Ca^{2+}]_o$ from physiological levels of 2 mM to 200 µM (Fig. 38*A*,*B*, $n = 4$) and decreased when $[Ca^{2+}]_o$ was increased to 20 mM (Fig. 38*C*,*D*, $n = 6$). Increased current amplitudes in low $[Ca^{2+}]_o$ were probably due to an increased frequency of channel opening (Fig. 38*F*). La^{3+} at a concentration of 100 µM inhibited the histamine-induced currents at all potentials (Fig. 38*A*,*B*,*E*, $n = 4$), which is also typical of recombinant rTRPC6. Outside-out patch recordings (Fig. 38*D*, $n = 4$) revealed kinetics similar to channels formed by recombinant rTRPC6. Single-channel chord conductance was about 41 pS ($n = 3$). Preliminary results suggest that the proportion of long events (> 1 ms) is increased. However, future studies will be needed for a detailed statistical analysis. Like rTRPC6 currents, currents mediated by rTRPC6-5 could be activated by OAG (50 µM) in whole-cell (Fig. 38*E*, $n = 4$) and single-channel experiments (Fig. 38F, $n = 2$).

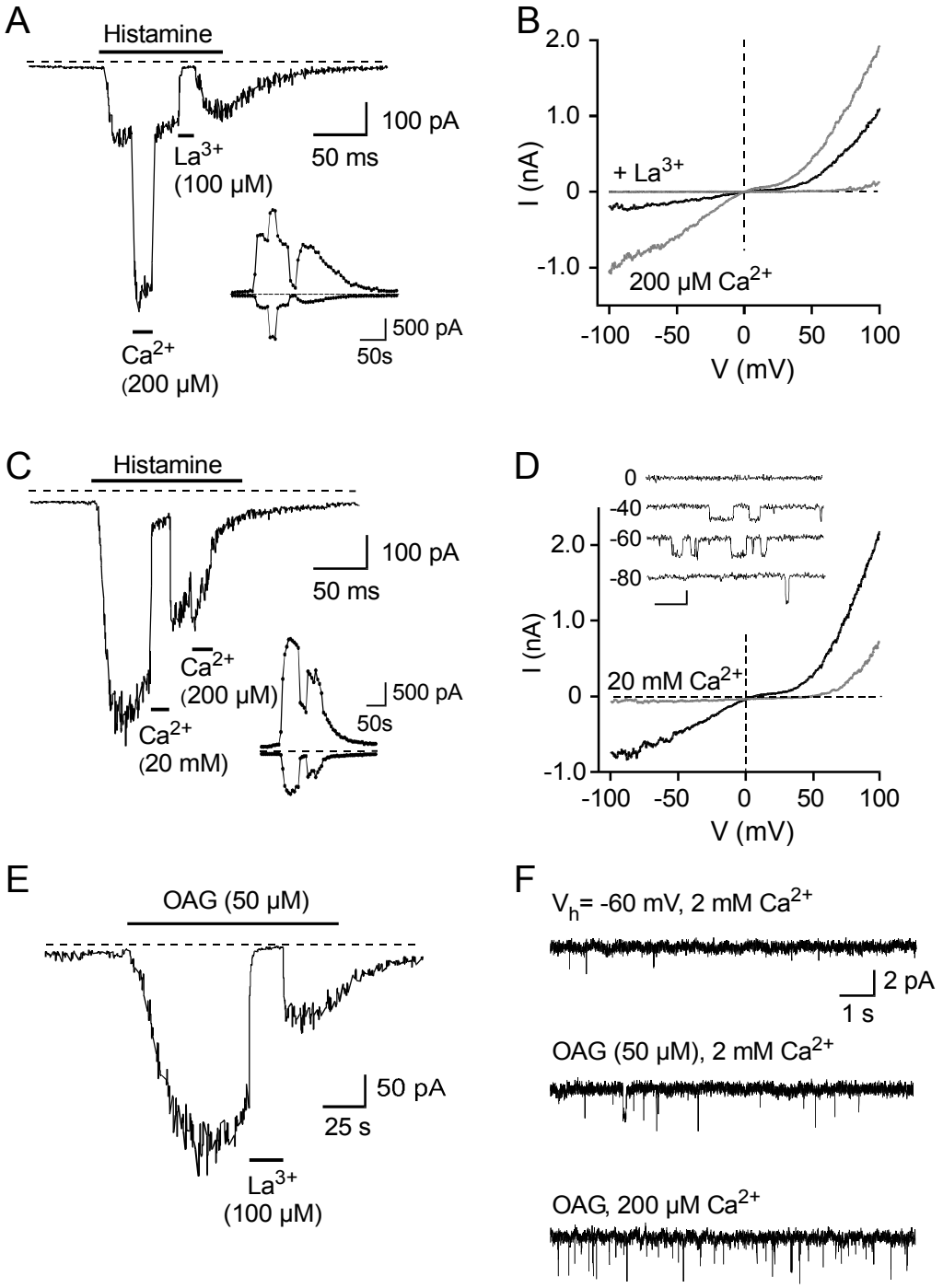

Fig. 38: **Currents carried by chimaeric TRPC6-5.** *A*,*C*,*E*: Whole-cell currents in TRPC6-5-expressing HEK293 cells at -60 mV elicited by histamine (100 µM, *A,C*) or OAG (*E*). Effects of decreasing (*A*) or increasing $[Ca^{2+}]_o$ (*C*), and of La^{3+} (*A*,*E*) are shown. *A*,*C*: *Inset*: corresponding currents at -100 or +100 mV. *B*: *I-V* relationships of the histamine-induced current in *A* in 2 mM and 200 µM Ca_o^{2+}-containing solutions, or in the presence of La^{3+}. *D*: *I-V* relationships of the HA-induced current in *C* in 2 mM and 20 mM Ca_o^{2+}-containing solutions. *Inset*: single-channel recordings obtained from HA-stimulated outside-out patches at the indicated potentials. *Scale bar*: 20 ms, 2 pA. *F*: Current traces recorded in outside-out patches at a membrane potential of -60 mV, before (*upper trace*) or during (*middle and lower traces*) application of OAG (50 µM), in 2 mM (*middle trace*) or 200 µM (*lower trace*) Ca_o^{2+}-containing solutions.

In conclusion, chimaeric TRPC6-5 was found to form receptor-activated cation channels, with properties indistinguishable from those of recombinant rTRPC6, but clearly distinct from those of recombinant mTRPC5 (see above). Obviously, to establish a TRPC6 phenotype, the N-terminal parts and transmembrane core of the TRPC6 protein are sufficient, whereas the C-terminal region of TRPC6 does not appear to make a major contribution to the channel properties. Future studies will have to clarify exactly which parts of the TRPC channel proteins are important for determining their distinct biophysical and regulatory properties.